


Dynamics of the major plinian eruption of Samalas in 1257 A.D. (Lombok, Indonesia)

Céline M. Vidal¹  · Jean-Christophe Komorowski¹ · Nicole Métrich¹ ·
Indyo Pratomo² · Nugraha Kartadinata³ · Oktory Prambada³ · Agnès Michel¹ ·
Guillaume Carazzo^{1,4} · Franck Lavigne⁵ · Jessica Rodysill⁶ · Karen Fontijn^{7,8} · Surono⁹

Received: 2 February 2015 / Accepted: 23 July 2015 / Published online: 8 August 2015
© Springer-Verlag Berlin Heidelberg 2015

Abstract The 1257 A.D. caldera-forming eruption of Samalas (Lombok, Indonesia) was recently associated with the largest sulphate spike of the last 2 ky recorded in polar ice cores. It is suspected to have impacted climate both locally and at a global scale. Extensive fieldwork coupled with sedimentological, geochemical and physical analyses of eruptive products enabled us to provide new constraints on the stratigraphy and eruptive dynamics. This four-phase continuous eruption produced a total of 33–40 km³ dense rock equivalent (DRE) of deposits, consisting of (i) 7–9 km³ DRE of pumiceous plinian fall products, (ii) 16 km³ DRE of pyroclastic density current deposits (PDC) and (iii) 8–9 km³ DRE of co-PDC ash that settled over the surrounding islands and was identified as far as 660 km from the source on the flanks of Merapi volcano (Central Java). Widespread accretionary lapilli-rich deposits provide evidence of the occurrence of a

violent phreatomagmatic phase during the eruption. With a peak mass eruption rate of 4.6×10^8 kg/s, a maximum plume height of 43 km and a dispersal index of 110,500 km², the 1257 A.D. eruption stands as the most powerful eruption of the last millennium. Eruption dynamics are consistent with an efficient dispersal of sulphur-rich aerosols across the globe. Remarkable reproducibility of trace element analysis on a few milligrammes of pumiceous tephra provides unequivocal evidence for the geochemical correlation of 1257 A.D. proximal reference products with distal tephra identified on surrounding islands. Hence, we identify and characterise a new prominent inter-regional chronostratigraphic tephra marker.

Keywords Samalas 1257 A.D. · Plinian eruption · Caldera-forming eruption · Phreatomagmatic eruption · Eruptive dynamics · Trace element analysis

Editorial responsibility: S. Self

Electronic supplementary material The online version of this article (doi:10.1007/s00445-015-0960-9) contains supplementary material, which is available to authorized users.

✉ Céline M. Vidal
vidal@ipgp.fr

¹ Institut de Physique du Globe, Sorbonne Paris-Cité, CNRS UMR-7154, Université Paris Diderot, 1 rue Jussieu 75238, Paris, Cedex 05, France

² Museum of Geology, Badan Geologi, Jl. Diponegoro 57, 40122 Bandung, Indonesia

³ Center of Volcanology and Geological Hazards Mitigation, Badan Geologi, Jl. Diponegoro 57, 40122 Bandung, Indonesia

⁴ Observatoire Volcanologique et Sismologique de la Martinique, Institut de Physique du Globe, Mome des Cadets, 97250 Fonds Saint-Denis, Martinique, FWI

⁵ Laboratoire de Géographie Physique UMR 8591, Université Paris 1 Panthéon-Sorbonne, 1 Place Aristide Briand, 92195 Meudon, France

⁶ Department of Geological Sciences, Brown University, Providence, RI 02912, USA

⁷ Department of Earth Sciences, University of Oxford, South Parks Road, Oxford, OX1 3AN, UK

⁸ Department of Geology and Soil Science, Ghent University, Krýgslaan 281-58, 9000 Ghent, Belgium

⁹ Badan Geologi, Jl. Diponegoro 57, 40122 Bandung, Indonesia

Introduction

Large explosive eruptions can discharge tens to thousands of cubic kilometres of finely fragmented magma and large amounts of associated sulphur and halogen gases into the atmosphere, on timescales of a few hours to days (e.g. Self 2006; Schmidt and Robock 2015). In the past, such infrequent but high-impact events have had devastating consequences both locally and at a global scale (Miller and Wark 2008). In recent years, the potential impact of volcanic eruptions on global climate with major implications has been the subject of intense research (e.g. Robock 2000; Schneider et al. 2009; Timmreck 2012).

Volcanic sulphate spikes recorded in polar ice cores attest to a powerful eruption that took place ca. 1257 or 1258 A.D., corresponding to the largest volcanic sulphur release to the stratosphere of the past 2000 years (Palais et al. 1992; Zielinski et al. 1994; Gao et al. 2008; Sigl et al. 2014). Computer modelling by Sigl et al. (2014) suggests that 170 Mt of SO₂ would be required to produce the observed sulphate spikes in Antarctic ice cores. This amount is greater than the 45 Mt of SO₂ estimated for the 1815 Tambora eruption and the 100 Mt of SO₂ associated with a large eruption that occurred in the late 1450s A.D. The latter is commonly associated with the Kuwae eruption in Vanuatu (e.g. Plummer et al. 2012; Cole-Dai et al. 2013; Sigl et al. 2013), although a firm attribution is not possible due to another spike dated 1452–1453 A.D. Furthermore, Miller et al. (2012) suggested that the 1257 A.D. eruption might have played a role in triggering the Little Ice Age, along with other stratospheric volcanic injections from eruptions in the thirteenth and fifteenth centuries. On the basis of their reconstruction of tree-ring chronologies for North America, Gennaretti et al. (2014) show evidence for a prolonged climatic shift to cooler temperatures following a series of thirteenth century eruptions and primarily after the 1257 A.D. eruption of Samalas. They further suggest that this marked the end of the Medieval Climate Anomaly and the onset of the Little Ice Age in northeastern America.

The search for the volcanic source responsible for the high sulphate spike associated with the 1257 A.D. event (1.6 times higher than the spike associated with the 1815 Tambora eruption, according to Sigl et al. 2014) has been inconclusive for years given that the amount of magma necessary to release such a quantity of aerosols was estimated at 200–800 km³ (Oppenheimer 2003) based on an empirical relationship between sulphur yields and the magnitude of corresponding eruption. Oppenheimer (2003) thus mentioned a ‘super-eruption’, but also suggested that the 1258–1259 A.D. sulphate-rich ice-core layers could result from the combined effects of a smaller volume of intermediate to silicic magma enriched in sulphur and the accumulation of a pre-eruptive sulphur-rich vapour phase, as observed for the eruptions of Cosingüina in 1835 (Longpré et al. 2014) and Pinatubo in 1991 (Gerlach et al. 1996). On the basis of field data on tephra dispersion and stratigraphy, preliminary eruptive dynamics data, radiocarbon dates, as well as critical interpretation of local and European medieval historical chronicles, Lavigne et al. (2013) recently identified this major event as the mid-thirteenth century caldera-forming eruption of Mt Samalas, on Lombok Island, Indonesia.

Lombok is located in the eastern Sunda arc (Fig. 1a), in a tectonic setting associated with the northward subduction of the Indo-Australian plate beneath the Eurasian plate at ca. 7 cm/year (Simons et al. 2007). The active volcanic centre of Lombok is the Central Lombok Volcanic Complex (CLVC, Fig. 1b) that is located at ca. 165 km above the Benioff zone. The CLVC is composed of (i) the large stratocone of Rinjani (3726 m a.s.l.) that is thought to have erupted last in 2550±50 B.P. (Nasution et al. 2004), producing the Rinjani Pumice, a sub-plinian pumice fall deposit of ca. 0.3 km³ dense rock equivalent (DRE); (ii) the 6.5×8-km-wide Samalas caldera resulting from the 1257 A.D. plinian eruption (Lavigne et al. 2013), with walls ranging from 700 to 2800 m in height and that hosts the 200 m deep Segara Anak Lake (Fig. 1b); and (iii) the active Barujari cone emerging 320 m above the lake that has produced lava flows and minor tephra falls during the 15 historical eruptions recorded since 1847 (Global Volcanism Program 2014). A sub-plinian event

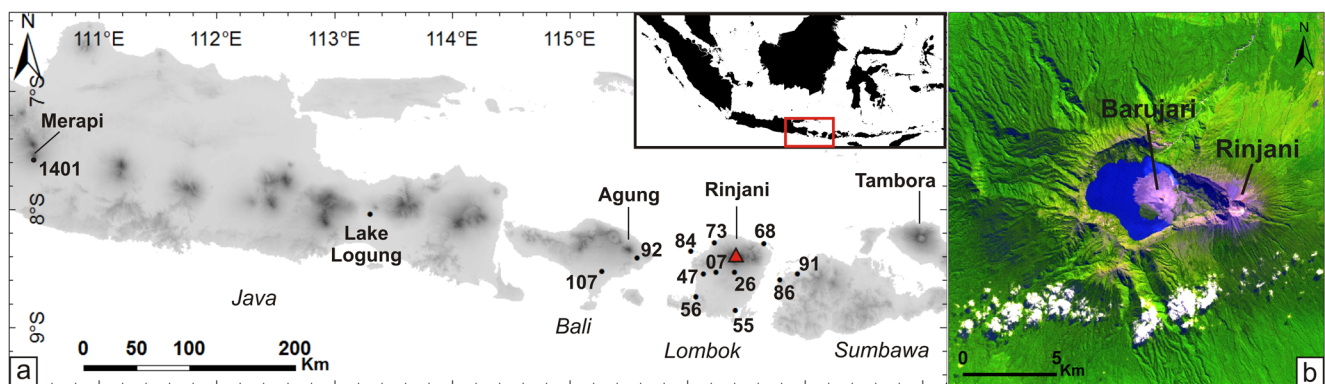


Fig. 1 a Overview of Lombok and Lesser Sunda arc islands in South Indonesia. Numbers refer to localities represented in stratigraphic logs of Fig. 2 ('RIN13' is omitted for brevity). b ASTER false colours image of Samalas caldera and Segara Anak Lake, with Rinjani and Barujari volcanoes (NASA)

occurred between 5990 ± 50 and 2550 ± 50 B.P. (Nasution et al. 2004, 2010) from a lateral vent located on the eastern flanks of Rinjani and produced the Propok Pumice deposit (0.1 km^3 DRE). Several scoria flow and fall deposits dated by Nasution et al. (2004) at $11,980\pm 40$, $11,940\pm 40$, 6250 ± 40 and 5990 ± 50 B.P. as well as pre-1257 A.D. thick scoria fall deposits that crop out on the N flank of the caldera were produced either by Rinjani or Samalas. The diversity of the volcanic products of the CLVC is representative of a large spectrum of compositions and eruptive styles, from effusive/violent strombolian to major plinian events. The 1257 A.D. caldera-forming eruption of Samalas was the most violent Holocene event of the CLVC. It was first recognised by Takada et al. (2003) and Nasution et al. (2004), who dated the caldera formation at 1210–1260 A.D., and estimated a total erupted volume of 10 km^3 DRE. Lavigne et al. (2013) not only associated this major eruption to the great mid-thirteenth century stratospheric dust veil (Stothers 2000; Oppenheimer 2003), but also estimated a total volume of ca. $40\pm 3\text{ km}^3$ DRE, suggesting that the 1257 A.D. eruption of Samalas was one of the largest of the past millennium.

In this paper, we present a significantly refined and revised stratigraphy for the 1257 A.D. eruption based on new extensive field work and laboratory analyses, which modifies the results of Lavigne et al. (2013). We rely on new and extensive trace element geochemical fingerprinting to successfully correlate the 1257 A.D. tephra deposits of Samalas over at least 660 km downwind from source. In particular, we discuss the discovery of several phreatomagmatic fallout units, very distal mobile turbulent dilute pyroclastic density current (PDC) deposits and voluminous plinian fallout units. This work also provides an opportunity to test new data processing protocols (e.g. Bonadonna and Costa 2013) to quantify the eruptive dynamics of a major plinian eruption. Our revised data on eruption magnitude and intensity (Pyle 2000) bears important implications to understand the potential regional and global climate impacts of one of the largest eruptions of the Holocene.

Stratigraphy of the 1257 A.D. Samalas deposits

We have identified the deposits of the 1257 A.D. eruption of Samalas in more than 100 locations on Lombok, Sumbawa, Bali and Java islands during extensive fieldwork in May–June 2013 and September 2014 (GPS coordinates are reported in Online Resource 1, Table S1). We have obtained 12 new ^{14}C dates on charcoal and burnt wood from the different phases of the eruption (Online Resource 1, Table S2).

Proximal deposits

Most of the studied outcrops on Lombok are located from the NW to the SW of the caldera. Exposure is very limited to the N, NE and particularly to the S of the island as a result of

erosion and extensive farming. Proximal exposures (<15 km from the source) are lacking because of the strong erosion that affects the steep flanks of the caldera and the scarce access within Rinjani National Park. Medial deposits (100–135 km) on Bali were identified at several locations including on the flanks of Agung (Fig. 2, site RIN1392) based on the work of Fontijn et al. (2015), on Bratan and Batur volcanoes and in central Bali (Fig. 2, site RIN13107). The stratigraphic and sedimentologic characteristics of these units, including a systematic decrease of grain size with distance from the source, correlate well with those of the westernmost deposits in Lombok at site RIN1384 (Fig. 2). Deposits W and SW of Rinjani can be easily recognised as they are the most widespread, thickest and located just below the current soil horizon. However, SE and E of the caldera as well as in western Sumbawa island, the light tan biotite-rich 1815 Tambora co-ignimbrite fine ash fall deposit (unit F5 of Sigurdsson and Carey 1989) forms a prominent regional stratigraphic marker just below the modern soil and above the paleosol overlying the 1257 A.D. deposits (Fig. 2, sites RIN1368, RIN1384, RIN1386, RIN1391 and RIN1355).

Based on diagnostic sedimentary, stratigraphic and physical features of the deposits, we divide the 1257 A.D. eruption into four major phases characterised by specific processes and deposits.

Phase P1

The eruption started with the emplacement of a thin (3 cm at 24 km distance) dark grey lithic-rich (i.e. accidental clasts) fine ash layer over ca. 400 km^2 in the NW of Lombok during a phreatic opening phase (e.g. Fig. 2, outcrop RIN1373). The magmatic part of the eruption started with the emplacement of the first thick and widespread pumice fallout unit (P1-PF) that mantles topography throughout a large part of Lombok. This prominent loose unit is lithic-rich and consists of white highly vesicular low density, occasionally fibrous pumice ($390\pm 80\text{ kg/m}^3$, see method in Online Resource 2). P1-PF is reversely graded and generally shows enrichment in lithic clasts towards the top. However, the first centimetres of the unit are enriched in fine-grained dark lithic clasts giving the deposit a diagnostic salt-and-pepper granular appearance. The finest fractions are rich in free plagioclase and amphibole crystals that are also the dominant phases in the highly vesicular white pumice clasts. The P1-PF deposit is coarse grained and generally poorly sorted downwind on Lombok, except at a few outcrops (e.g. Fig. 2; outcrop RIN1384). This unit extends furthest downwind to Bali, 126 km W of the source where it is 8 cm thick (Fig. 2, outcrop RIN13107). Its last footprint upwind is on the East coast of Lombok, where it is 8 cm thick 33 km from the source (Fig. 2, outcrop RIN1368). It was not observed 50 km SW from the source at location RIN1355 (Fig. 2), the farthest crosswind outcrop of the 1257 A.D. units.

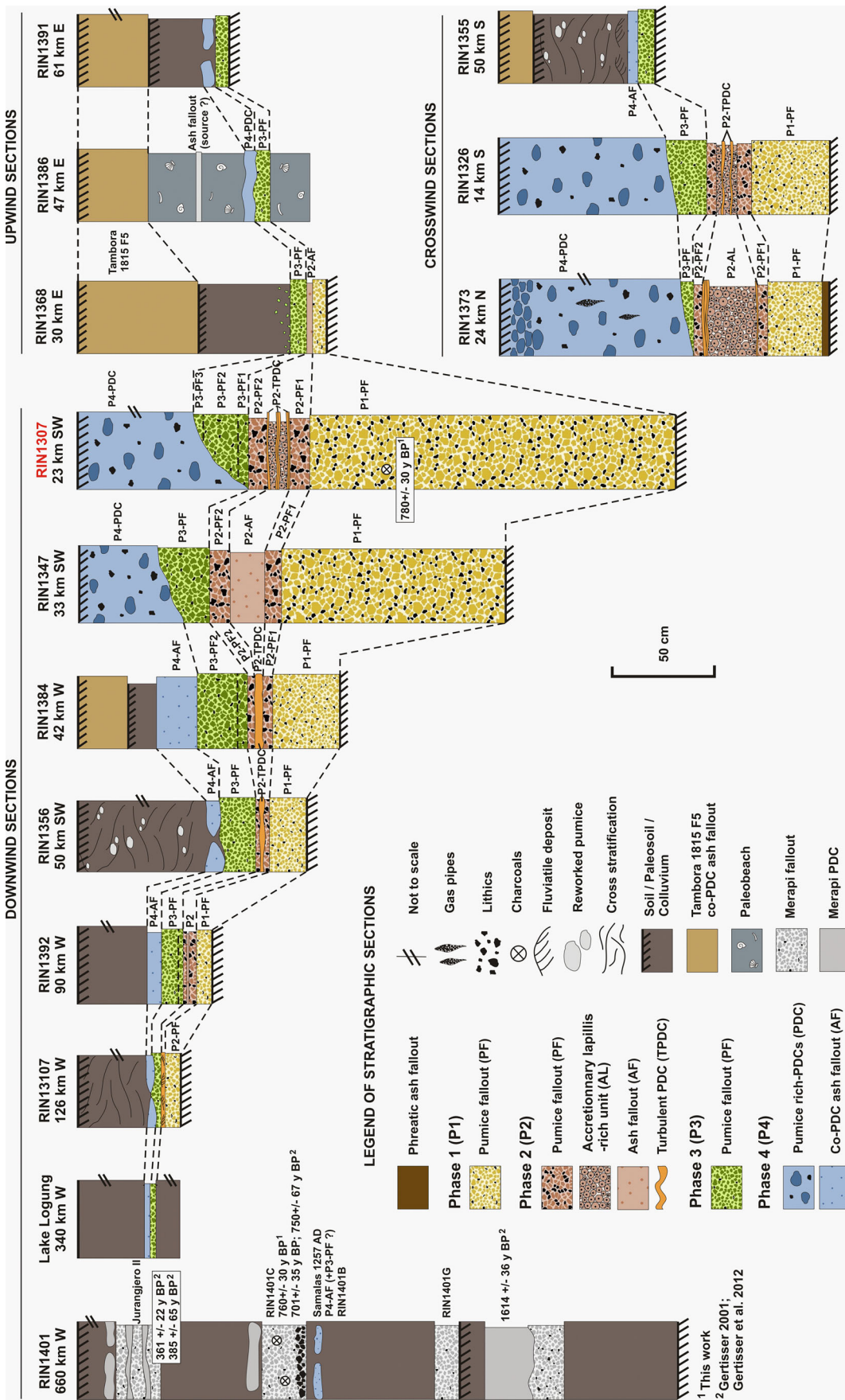


Fig. 2 Stratigraphic logs of representative sections of deposits of 1257 A.D. Samalás eruption from Lombok, Sumbawa, Bali and Java. See Fig. 1a for location of outcrops. RIN1307 is the type section displaying the entire stratigraphy. Jurangero II Merapi tephra at site RIN1401 was studied by Gertisser (2001) and Gertisser et al. (2012). PDC pyroclastic density current

The P1-PF unit often contains archaeological ceramic artefacts and small charcoal fragments towards the base that we dated at 1210–1281 cal A.D. (Online Resource 1, Table S2).

Phase P2

This phase begins with the emplacement of a fine-grained, normally graded pumice fallout deposit (P2-PF1) with abundant lithic clasts and light greyish moderately vesicular pumice. The gradational contact between P1-PF and P2-PF1 and the lack of erosion or remobilised pumice deposits on top of the PF1 unit suggest that there was no time break between the deposition of the phase P1 unit and the overlying phase P2 unit.

Unit P2-PF1 is overlain by a variably thick (14–50 cm, Fig. 2, outcrop RIN1373), massive, compact, very well sorted, very fine-grained ash-rich unit with abundant accretionary lapilli (P2-AL) that are up to 0.5–2 cm in diameter. In several localities, this unit consists of several layers that are intercalated and partly truncated by several, wavy-laminated, coarse ash-rich, moderately sorted, erosive layers of variable thickness (0.5 to 3 cm). We interpret these wavy-bedded layers as resulting from the emplacement of distal dilute turbulent PDC deposits (P2-TPDC) (Fig. 2, outcrops RIN1307, RIN1373, RIN1326; Fig. 3f, g). The wavy layers are richer in lithic clasts but contain scattered 1–4 cm sized armoured pumice clasts (i.e. pumice core coated with concentric laminae of blue-grey fine ash) as well as scattered accretionary lapilli. These P2-AL and P2-TPDC units can be found over a widespread area up to 25 km NW and SW from the caldera (Fig. 3f). They often have a prominent characteristic blue-grey colour with local orange oxidation marks. This observation suggests that they largely consist of altered material from the hydrothermal system (reduced iron sulphides, e.g. pyrite, iron oxides and clay minerals). The P2-AL units contain abundant solidified casts of wood fragments as well as burnt wood fragments dated at 1157–1264 cal A.D. (Online Resource 1, Table S2). The variable thickness of the blue accretionary lapilli-rich P2-AL unit, the preferential occurrence of the accretionary lapilli-rich facies in the vicinity and within pre-eruption deep valleys and the thin wavy laminations suggest that it might correspond to a locally more concentrated, distal low-energy facies of the associated P2-TPDC units emplaced in the presence of abundant water vapour. At some localities, a massive and compact brownish ash fallout unit (P2-AF) containing small pumice clasts is observed instead of the succession of P2-AL and P2-TPDC layers (Fig. 2, outcrops RIN1347, RIN1384, RIN1392 and RIN1368).

At several localities to the W and SW, we find a brownish fine to coarse ash unit (8 to 16 cm thick) that shows a characteristic variable and undulating thickness and contains accidental and sub-rounded pumice clasts towards the base. This unit strongly erodes the underlying P2-PF1 and P1 units. These undulations form a series of at least three U-shaped channels,

the axes of which are oriented roughly NS with N5° W–N6° E and N2° W–N6° E (declination set 13° W). This orientation is perpendicular to the EW direction that primary PDCs would have followed radially away from the caldera. The infilling of the channels by the remainder of the pumice fallout units of the P2 and the P3 phases indicates that the channels formed during the phreatomagmatic phase P2. We interpret these U-shape channels to be erosional furrows caused by the emplacement of P2-TPDC that were deflected upon their interaction with high topography that would have provided additional potential energy for the dilute PDCs that overpassed it. The PDCs were able to re-condense and likely experienced a second collapse from the lift-off cloud that formed above the high topography (Druitt et al. 2002). The collapsing PDCs were then partly confined by the deep valleys on the flanks of the Western volcanic complex. These dilute PDCs thus probably occurred before the caldera-collapse phase.

The P2 phase ends with the emplacement of a second grey pumice fallout unit (P2-PF2) that is moderately sorted, normally graded and composed of a mixture of whitish grey moderately vesicular pumice and abundant lithic clasts. This unit is more lithic rich, better sorted and finer grained than the basal P2-PF1 unit. It is characterised by a relatively widespread distribution and reaches up to 2 cm in thickness in eastern Bali (Fig. 2, outcrop RIN1392; Fig. 3b).

The P2-TPDC deposits can be observed on the Gili islands up to 41 km NW from the caldera (Fig. 2, outcrop RIN1384) and even up to 52 km SW towards the Western Lombok peninsula (Fig. 2, outcrop RIN1356). This implies that these TPDCs were highly energetic and mobile to cross over regions of elevated topography and travel up to 10 km over the Bali Sea. The alternation of relatively widespread pumice-rich fallout units with several turbulent mobile dilute PDCs and widespread very fine ash units containing abundant large accretionary lapilli suggests a highly energetic phreatomagmatic fragmentation process that involved mixing of magma with abundant external water at the vent during phase P2, as discussed further.

Phase P3

Phase P3 is characterised by the emplacement of the most widespread pumice fallout unit (P3-PF) of the entire eruption. P3-PF is divided into three sub-units (P3-PF1, P3-PF2 and P3-PF3 from base to top) that are gradational into each other and can be distinguished on the basis of their grain size, sorting and grading. P3-PF1 is a pinkish-oxidised, reversely graded, very poorly sorted and the most lithic rich of the P3 fallout units. P3-PF2 is normally graded, moderately sorted and the thickest of the three sub-units. P3-PF3 is normally graded, moderately sorted and the coarsest unit of the P3 deposits. The three units were observed together at three sites including the RIN1307 type locality (Fig. 2), although generally only P3-PF1 and/or

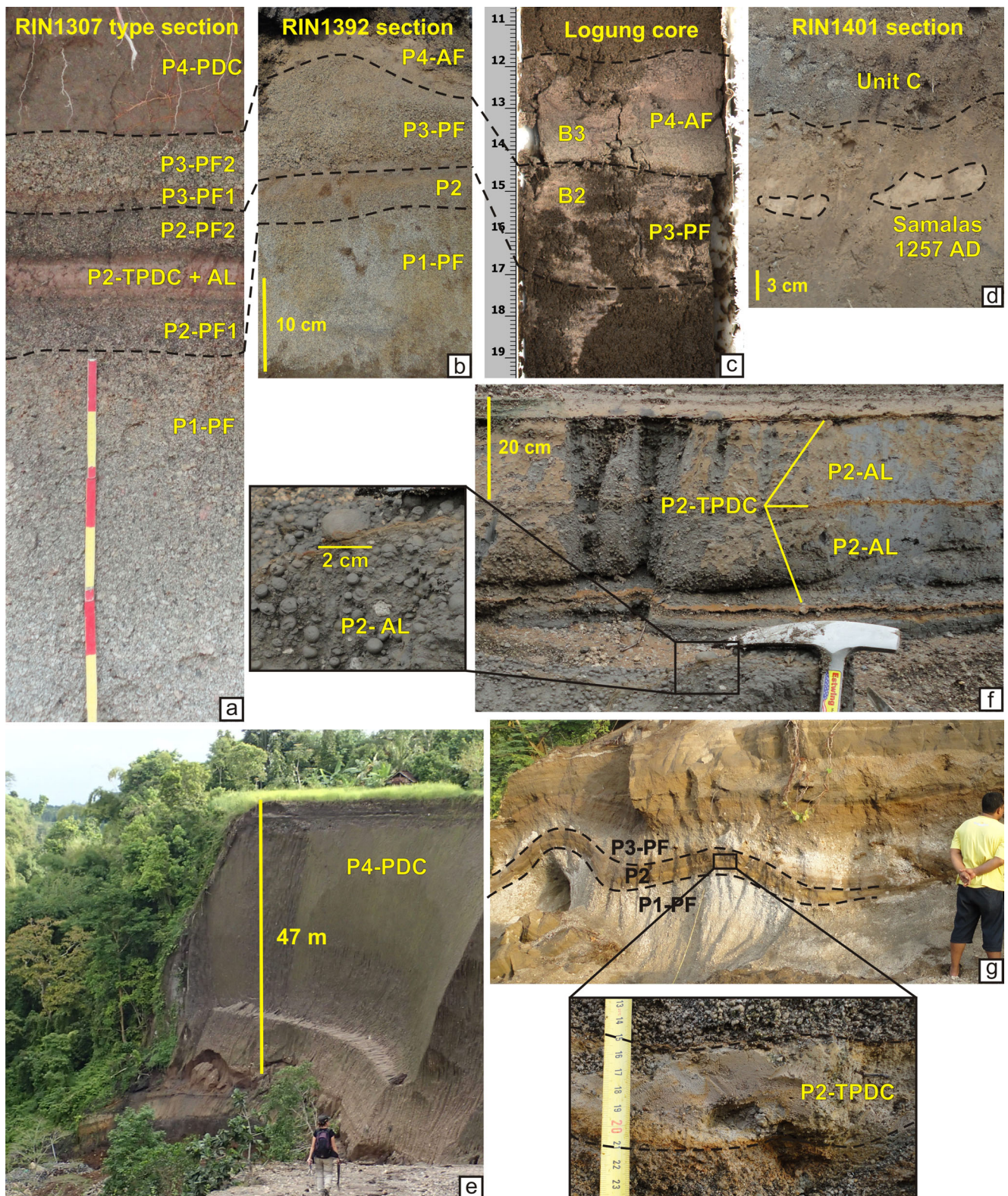


Fig. 3 **a–d** Representative pictures of outcrops of the 1257 A.D. Samalas deposits on Lombok, Bali, East and Central Java, respectively. See Figs. 1a and 2 for location and distance from the source. **e** PDC deposits emplaced during phase 4 filling the Sedau Valley, 25 km SW

from the source. **f** Turbulent PDC (P2-TPDC) and accretionary lapilli-rich (P2-AL) units emplaced during the phreatomagmatic phase P2, 25 km SW from the source. **g** Wavy-bedded P2-TPDC and P2-AL units, 17 km NW from the source

P3-PF2 are observed. The P3-PF units contain pumice clasts slightly less vesicular ($603 \pm 140 \text{ kg/m}^3$, Online Resource 2) and more texturally diverse (white to whitish grey colour, larger range of vesicularity, less fibrous vesicles) than the markedly fibrous and very low density white pumice clasts of P1-PF. There is a systematic decrease in the abundance of lithic clasts from the lower subunit P3-PF1 to the uppermost P3-PF3 subunit. We have traced the P3-PF unit 61 km upwind on Sumbawa Island where it is up to 7 cm thick (Fig. 2, outcrops RIN1386, RIN1391) and contains scattered pumice clasts of 3 cm in diameter, and up to 50 km crosswind on the southern coast of Lombok (Fig. 2, site RIN1355). At proximal localities, the P3-PF unit is thinner than the P1-PF unit because it has been eroded by a succession of PDCs of the subsequent phase P4 (Fig. 2, outcrops RIN1307, RIN1326, RIN1347 and RIN1373). However, in areas beyond the runout of PDCs, the P3-PF unit is often as thick as or thicker than the P1-PF unit (Fig. 2, outcrops RIN1368, RIN1384, RIN1356 and RIN1392).

Phase P4

In numerous locations covering a vast area to the N, SW, S and SE of the caldera, the pumice fallout units of phase P3 are directly overlain by a series of thick pumiceous PDC deposits (P4-PDC) that can reach cumulative thicknesses of up to ~50 m (Fig. 3e). We identified at least six distinct non-welded units that form extensive flat-topped valley-ponding sequences that fill all the deep valleys that radiate from the caldera in all directions. The emplacement of these PDCs was strongly controlled by the pre-eruption paleotopography. To the E and W, the PDCs were diverted by the high topography of the older volcanic complexes. The PDCs were channelled by two deep paleo-valleys oriented SE and SW and were able to reach distances of at least 28 km to the S and SW. These large drainage systems were developed as a geomorphologic response to the emplacement of an older voluminous and thick (>100 m) lobate and hummocky debris avalanche deposit that formed a major topographic barrier to the S.

The base of the lowermost PDC unit comprises an indurated, wavy-stratified, 10- to 13-cm-thick unit locally containing some rounded pumice clasts. The contact between the basal part of the P4-PDC sequence and the P3 fallout is formed by a laminated 0.5- to 1-cm-thick, indurated, wavy-bedded layer that is very rich in black indurated organic material. This basal unit is interpreted as having been deposited from a more dilute stratified high-energy current that caused very rapid wholesale combustion of the pre-eruption vegetation. This led to the formation of a carbon-rich aerosol that settled to form this indurated tar layer (e.g. Sparks et al. 2002; Voight et al. 2002; Bull et al. 2008; Scott et al. 2008). Several P4-PDC units show concentrations of large (>20 cm) pumice clasts towards the unit top as well as pumice lenses within the unit. The presence of U-shaped channels in the P4-PDC units with different orientations suggests that

PDCs also interacted locally with the pre-eruption topography and that the first PDCs followed pre-eruption river channels with different orientations.

We interpret the emplacement of these massive voluminous PDCs on all sides of the volcano as evidence for the wholesale collapse of the phase P3 eruption column and the climactic transition to the formation of the 6.5×8 -km-wide complex caldera (Fig. 1b). Field evidence indicates that pumice content markedly diminishes from the first basal PDC unit of phase P4 to the uppermost units that are darker in colour. This observation suggests that an important erosion of the crater occurred during the P4 phase that leads to the formation of a large caldera. These new conditions at the vent promoted the formation of a sustained low pyroclastic fountaining (Branney and Kokelaar 2002) in which entrainment and mixing of ambient air was insufficient to form a buoyant plume (Sparks and Wilson 1976).

The absence of pumice fallout units intercalated between the main P4-PDC units indicates that a vertical convective column was not able to re-establish itself after the emplacement of the first PDC units. The interaction of the primary low fountain collapse PDCs with topographic barriers led to the generation of a major lift-off cloud that was able to collapse and re-sediment to form secondary dilute PDCs (e.g. Druitt et al. 2002) that evidently were capable to cross the sea and form a thin unit associated with their tapering flow margins on the western coast of Sumbawa (Fig. 2, outcrop RIN1386).

The voluminous P4-PDCs reached the pre-eruption coast line and formed massive 10- to 35-m high cliffs of non-welded deposits primarily on the northern coast of Lombok but also to the SE in the straits separating Lombok from Sumbawa. The PDCs formed a major pyroclastic delta along the northern coast. Their entrance in the sea generated violent secondary phreatomagmatic explosions that produced a series of numerous turbulent dilute PDCs. These jetted in a pulsating manner from the sea entry point and carried pumiceous and lithic pyroclastic material that accumulated to build a large pumice littoral cone (Furukawa et al. 2005, 2014; Lavigne et al. 2013). The cliff face shows typical wavy bedding and cross-stratification with wavelengths of 1–2 m, as well as very well-developed planar bedding giving the deposits a marked stratification. The lithic clasts are diagnostically oxidised and are aligned in a sub-parallel manner. Following the deposition of the PDCs, secondary explosions likely continued for a long time as the coastal wave action eroded the deposits, exposing the hot PDC interior to seawater. The emplacement and sea entry of PDCs formed a large lift-off cloud that produced a widespread co-PDC ash fall deposit P4-PF, which is observed downwind and crosswind as a massive and compact tan to whitish very fine ash unit (Fig. 3b).

Distal deposits

We have successfully identified the 1257 A.D. tephra in two distal sites. Rodysill et al. (2012, 2013) identified a tephra

layer in a sediment core obtained from Lake Logung, on the flanks of Lamongan volcano (East Java) 340 km from source, at a core depth between 533.8 and 540.3 cm below the lake bottom. The date of 720 ± 25 B.P. (Rodysill et al. 2012; recalibrated with IntCal13 at 1256–1299 cal A.D., Online Resource 1, Table S2) on a sample of wood from a cumulative sediment depth of 491.4 cm (ca. 42.4 cm above the tephra layer) is consistent with deposition of this tephra during the 1257 A.D. eruption of Samalas.

Andreastuti (1999) and Andreastuti et al. (2000) have recognised, at different sites in East Java (e.g. Ijen, Bromo, Kelut), and particularly on the flanks of Merapi volcano, a very fine-grained ashfall unit containing highly vesicular pumiceous clasts. They interpret this layer as an inter-regional tephra unit that they name the Muntilan tephra. Given its sedimentologic characteristics, its eastward thickening trend and its bulk chemical composition that differs from Merapi tephra units above and below, they interpreted the Muntilan tephra as having originated from an unknown distal large eruption located further East in Java. For these authors, the age of the Muntilan tephra is not known precisely but is well bracketed on Merapi by radiocarbon age dates of 780 ± 50 B.P. (1157–1295 cal A.D., Online Resource 1, Table S2) and 783 ± 44 B.P. (1166–1285 cal A.D., Online Resource 1, Table S2) on charcoal from a PDC deposit above the Muntilan tephra (site 240, WK-4404; Andreastuti et al. 2000), and by a radiocarbon age of 1112 ± 73 B.P. (710–1037 cal A.D., Online Resource 1, Table S2) on charcoal from the Selo tephra below the Muntilan tephra (site 270, WK-5613; Andreastuti et al. 2000; Newhall et al. 2000). A fine ash deposit, which is compatible with the Muntilan tephra, was also identified by Gertisser et al. (2012) at different locations in a similar stratigraphic position. Given these data, we strongly suspect that at least some of the units regrouped under the name ‘Muntilan inter-regional tephra’ correspond to very distal fine ash from the 1257 A.D. eruption of Samalas. We studied a new outcrop on the flanks of Merapi (Fig. 2, section RIN1401) in the village of Kinarejo where we recognised Merapi tephra units from the last ca. 1500 years above and below a patchy unit of ash (Fig. 3d) resembling the published descriptions of the Muntilan tephra. This tephra consists of elongated rounded patches of compact yellowish very well-sorted, very fine ash occurring in a thick paleosol horizon. Although the primary thickness could not be measured, individual patches are 1 to 2.5 cm thick. These patches of fine ash are directly overlain by a laterally continuous prominent grey, loose, poorly sorted, normally graded coarse ash fall unit that is 0.12 to 0.22 m thick and that contains coarse accidental clasts at the base. Our new radiocarbon date for small charcoal flakes present in this unit at 760 ± 30 B.P. (1219–1284 cal A.D., Online Resource 1, Table S2; sample RIN-1401-CW1) confirms that it is slightly younger than the Muntilan tephra below. We thus consider this unit to be the 1257 A.D. Samalas tephra and rename it accordingly.

This new date closely matches the radiocarbon dates (Online Resource 1, Table S2) of 750 ± 67 B.P. (1154–1394 cal A.D., recalibrated using IntCal13; sample M96-112) and 701 ± 35 B.P. (1256–1390 cal A.D., recalibrated using IntCal13; sample M97-069) from Gertisser (2001) and Gertisser et al. (2012) that were sampled at a very nearby location (B3) in Kinarejo, in a PDC deposit that eroded into this grey fallout unit (sample RIN-1401-CW1). At this location, Gertisser (2001) and Gertisser et al. (2012) describe a stratigraphy that is very similar to that of RIN1401 (Fig. 2) in which the lowermost pumice-rich fallout unit is overlain by a 0.24-m-thick grey sandy erosive PDC unit containing abundant accidental clasts dated at 1614 ± 36 B.P. (381–543 cal A.D., recalibrated using IntCal13; sample M97-070). The thin normally graded pumice fallout unit (0.12 cm) that we observe above this older basal PDC unit and below the Muntilan tephra might correspond to the high-K andesites of the younger Kinarejo tephra described by Gertisser (2001, pp. 44–45) although this needs to be confirmed by geochemical analyses.

We discuss later the positive correlation of the trace element composition of juvenile pumice from fine ash from the Logung core and from site RIN1401 on Merapi with the reference 1257 A.D. tephra deposit on Bali and Lombok.

Geochemical and textural correlation of distal tephra

The bulk-rock and matrix glass chemistry of 1257 A.D. pumice from different grain size fractions were determined using analytical methods described in Online Resource 2.

Geochemistry of bulk pumice clasts

Major and trace elements were analysed in proximal and medial pumiceous clasts (>16 mm) of all phases of the 1257 A.D. eruption of Samalas that display a homogeneous trachydacitic composition (64.3 ± 0.3 wt% of SiO_2 and 7.7 ± 0.7 wt% of $(\text{Na}_2\text{O} + \text{K}_2\text{O})$, normalised to 100 % on anhydrous basis; Online Resource 1, Table S3).

Trace elements were also systematically measured on small quantities of pumice clasts manually selected from several grain size fractions from proximal, medial and distal tephra of the four phases of the 1257 A.D. eruption (P1, P2 and P3 pumice fallouts and P4 co-PDC ash fallout). A total of 31 analyses were performed by inductively coupled plasma-mass spectrometry (ICP-MS) on the 1257 A.D. samples (Online Resource 2). The entire dataset including the RSD values for each element is reported in Online Resource 1 (Tables S5 and S6). The representative compositions of the 1257 A.D. tephra from proximal and medial and from distal sites identified on Java (LOGB2, LOGB3 and RIN1401B samples) are given in Table 1.

Table 1 Average trace element compositions of proximal, medial and distal bulk tephra of the 1257 A.D. Samalas eruption

Tephra Section ^a	Samalas 1257 A.D.			Logung core				RIN1401B			
	RIN1307, RIN1386, RIN1392			Lake Logung				RIN1401			
Distance from source (km)	23–90			340				660			
Region	Lombok, Sumbawa, Bali			East Java				Central Java			
	Average (22) ^b	SD (ppm) ^c	RSD (%) ^d	Average (8)	SD (ppm)	RSD (%)	%Error ^e	One analysis	SD (ppm)	RSD (%)	%Error
Li (ppm)	26.8	0.9	3.4	25.9	nd	nd	3.5	28.5	0.3	1.1	6.0
Ba	822	31	3.7	839	17	2.1	2.0	855	3	0.4	4.0
Ce	54.7	2.0	3.6	53.7	1.2	2.2	1.9	52.8	0.2	0.4	3.4
Cs	3.7	0.1	3.9	3.9	0.10	2.6	6.6	4.48	0.03	0.7	22
Co	5.7	1.0	17	4.2	0.4	10	26	4.0	0.1	2.2	29
Dy	4.48	0.16	3.5	4.53	0.07	1.6	1.0	4.68	0.08	1.7	4.4
Er	2.94	0.10	3.4	2.99	0.05	1.8	1.9	3.05	0.03	0.9	3.8
Eu	1.21	0.05	4.2	1.2	0.02	1.9	1.3	1.33	0.01	0.9	10.5
Hf	6.8	0.3	4.3	6.7	0.19	2.9	1.4	7.5	0.1	1.4	9.6
La	26.9	1.0	3.8	27.8	0.53	1.9	3.2	29.4	0.2	0.6	9.2
Lu	0.512	0.017	3.3	0.524	0.008	1.5	2.3	0.54	0.01	1.6	5.0
Nb	10.7	0.4	3.9	10.9	0.23	2.1	1.3	11.8	0.06	0.5	9.8
Nd	23.19	0.91	3.9	23.5	0.36	1.5	1.5	24.5	0.2	0.9	5.8
Pb	15.4	1.0	6.6	na	nd	nd	nd	14.8	0.2	1.4	3.8
Pr	6.15	0.24	3.8	6.3	0.1	1.8	1.8	6.6	0.07	1.0	6.6
Rb	101.8	4.1	4.0	108.0	2.4	2.2	6.1	102.5	0.6	0.6	0.7
Sm	4.8	0.2	3.6	4.81	0.09	1.9	1.0	5.0	0.1	2.7	5.3
Sr	268	18	6.6	248	11	4.4	7.7	276.3	0.8	0.3	3.0
Ta	0.73	0.03	3.4	0.7	0.02	2.7	3.2	0.743	0.004	0.6	1.5
Tb	0.73	0.03	3.6	0.74	0.01	1.5	1.3	0.75	0.01	1.2	3.3
Th	11.2	0.4	3.6	11.0	0.3	2.3	1.7	11.6	0.1	0.6	3.3
U	2.78	0.10	3.7	2.8	0.11	3.7	2.6	2.98	0.02	0.6	7.5
V	32.1	7.9	25	27.5	1.4	5	14	31.3	0.4	1.4	2.6
Y	25.2	0.85	3.4	25.8	0.50	1.9	2.3	24.8	0.10	0.4	1.5
Yb	3.25	0.11	3.4	3.31	0.06	1.8	1.8	3.44	0.03	0.9	5.7
Zr	284.0	12.3	4.3	282	4.8	1.7	0.8	294	1.9	0.7	3.5
		$\pm 1\sigma$			$\pm 1\sigma$		%Error		$\pm 1\sigma$		%Error
Nb/Zr	0.038	0.002		0.039	0.001		2.1	0.0401	0.0003		6.1
Th/Ta	15.3	0.8		15.5	0.6		1.6	15.6	0.1		1.8
Nb/U	3.9	0.2		3.8	0.2		1.3	4.0	0.0		2.2
La/Nb	2.5	0.1		2.6	0.1		2.0	2.5	0.0		0.5
Rb/Nb	9.5	0.5		9.9	0.3		4.8	8.7	0.1		8.3
Th/Yb	3.4	0.2		3.3	0.1		3.4	3.4	0.0		2.2
Ba/Th	73.5	3.8		76.3	2.4		3.8	74.0	0.5		0.7
La/Sm	5.7	0.3		5.8	0.2		2.2	5.9	0.2		3.7

na not analysed, nd not determined

^a See Figs. 1, 2 and 3 for geographic location and pictures of the deposits

^b The number of analyses (*N*) averaged is indicated in parentheses

^c SD is the standard deviation. For single measurements, the SD values are derived from the count numbers

^d RSD (%) is the relative standard deviation ($100 \times \sigma / \text{mean}$)

^e %Error is given by $[100 \times (\text{unknown value} - \text{Mean}_{\text{Rin}}) / \text{Mean}_{\text{Rin}}]$, expressed as absolute values, where Mean_{Rin} is the average of 22 analyses of the 1257 A.D. proximal, medial and distal tephra; the unknown values refer to Logung core tephra, or to the sample RIN1401B attributed to the 1257 A.D. tephra on the flanks of Merapi

The data reproducibility was checked by repetitive measurements, during three different analytical sessions, on two aliquots of medial (RIN1392E) and distal (LOGB2 and LOGB3) 1257 A.D. tephra. For aliquots of >10 mg of these two samples, the RSD values range between 1 and <5 % (except for Pb in LOGB3 sample, possibly due to external pollution). Decreasing the sample mass down to 4–6 mg slightly increases the RSD values (from 3 to 7 %) in the grain size fractions 1–0.5 and 0.5–0.25 mm (RIN1392E; Online Resource 1, Table S5). We underscore that we performed analyses on quantities as low as 3.3 mg (RIN1392E) and 4.4 mg (LOGB3). The calculated %errors range between 1 and 5 %. The main exceptions are Co (up to 20 %) and V to some extent, for which the variability can be higher because of the drastic effect of the presence of even the most minute titanomagnetite microlites.

The pattern of trace element abundances demonstrates a very good match between (i) the 1257 A.D. Samalas pumice clasts from the P1, P2, P3 and P4 phases; (ii) the three grain size fractions; and (iii) the proximal and the medial tephra from Bali (RIN1392), as illustrated in Fig. 4a. Regardless of the grain size fractions used, the 1257 A.D. tephra display on average (22 analyses) similar ratios of incompatible trace elements such as Nb/Zr (0.038 ± 0.002), Th/Ta (15.3 ± 0.8), Nb/U (3.9 ± 0.2), Th/Yb (3.4 ± 0.2), La/Nb (2.5 ± 0.1), Rb/Nb (9.5 ± 0.5) and Ba/Th (73.5 ± 3.8).

Our analyses unambiguously confirm the presence of the 1257 A.D. tephra in the Logung core (LOGB2 and LOGB3 samples; East Java) and as far as 660 km from the source on the flanks of Merapi (RIN1401B sample; Central Java). In the LOGB2 and LOGB3 samples, the %error values range from 1 to ≤ 3.5 % for most elements and reach 6–8 % for Cs, Rb and Sr (Table 1). For the sample RIN1401B from the flanks of Merapi, the %error values are slightly higher (5–10 %; Table 1) because of the low quantity of available material and the total mass (2.2 mg) of the aliquot analysed.

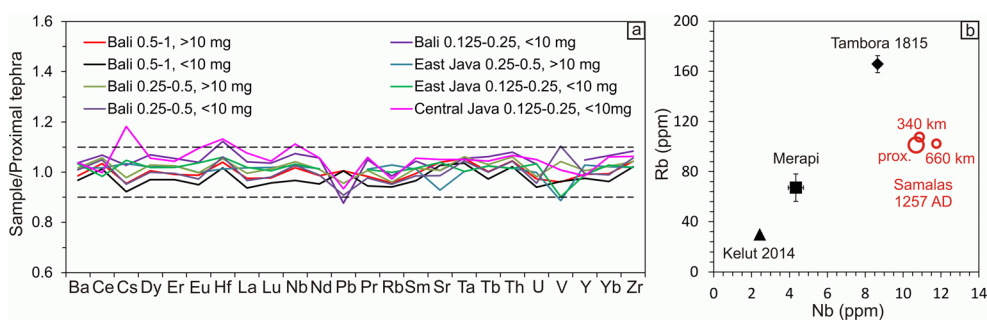


Fig. 4 **a** Trace element concentrations of tephra of the 1257 A.D. Samalas eruption on Bali (site RIN1392), East Java (Logung core) and Central Java (flanks of Merapi, site RIN1401) normalised to the average element concentrations of the proximal tephra from all phases on Lombok (site RIN1307). Data are reported in Table 1. Within the error bar, proximal, medial and distal tephra are chemically homogeneous, regardless of the grain size fractions. For each trace element pattern, we indicated the location, the grain size (0.5–1.0, 0.25–0.5 and 0.125–0.25)

Figure 4b shows that the 1257 A.D. distal tephra strongly differs from the K-rich products of the 1815 Tambora eruption, which display significantly higher Nb/Zr (0.049 ± 0.003), La/Nb (4.8 ± 0.2) and Rb/Nb (19.1 ± 0.9) ratios (Online Resource 1, Tables S5 and S6). Furthermore, the chemical signature of the 1257 A.D. distal tephra is markedly different from that of tephra erupted in the last 1000 years by neighbouring volcanoes such as Merapi and Kelut. In particular, the RIN1401B tephra sampled on the flanks of Merapi is diagnostic of pure 1257 A.D. products and has not been mixed with other Merapi tephra at RIN1401 section (Online Resource 1, Tables S5 and S6).

Matrix glasses

Matrix glasses of proximal and distal pumiceous 1257 A.D. tephra of all eruptive phases were analysed by EPMA for major element compositions (Online Resource 2). Analyses are reported in Table S7 of Online Resource 1. Matrix glasses share comparable trachy-dacitic compositions. However, we stress that those of P1-PF have a slightly but significantly lower SiO₂ content calculated on anhydrous basis (68 ± 0.5 wt%) than those of P3-PF and P4-AF (>70 wt%). This reflects textural differences in the pumice textures with the systematic presence of sub-micrometric crystals of feldspar, pyroxene and Fe-Ti oxide that grew as a result of magma ascent and degassing, specifically in P3 and P4 tephra (Fig. 5d–i).

Textural identification of phases of the eruption in distal tephra

Sedimentological analyses of the tephra unit in the Logung core evidenced two layers B2 and B3 (Fig. 3c) of very fine-grained pumice (Fig. 5c) that correspond to fallout deposition from two subsequent phases of the eruption. Tephra deposited

in millimetres and the sample mass (> or <10 mg). **b** Rb vs. Nb plot of 1257 A.D. Samalas proximal tephra (Lombok, Sumbawa and Bali), Logung core tephra and RIN1401B tephra sampled on the flanks of Merapi compared with historical tephra from Merapi (1401C, 1401G) at site RIN1401, 2014 Kelut eruption tephra and 1815 Tambora F5 co-PDC tephra (Sigurdsson and Carey 1989). Error bars are reported (Online Resource 1, Table S5)

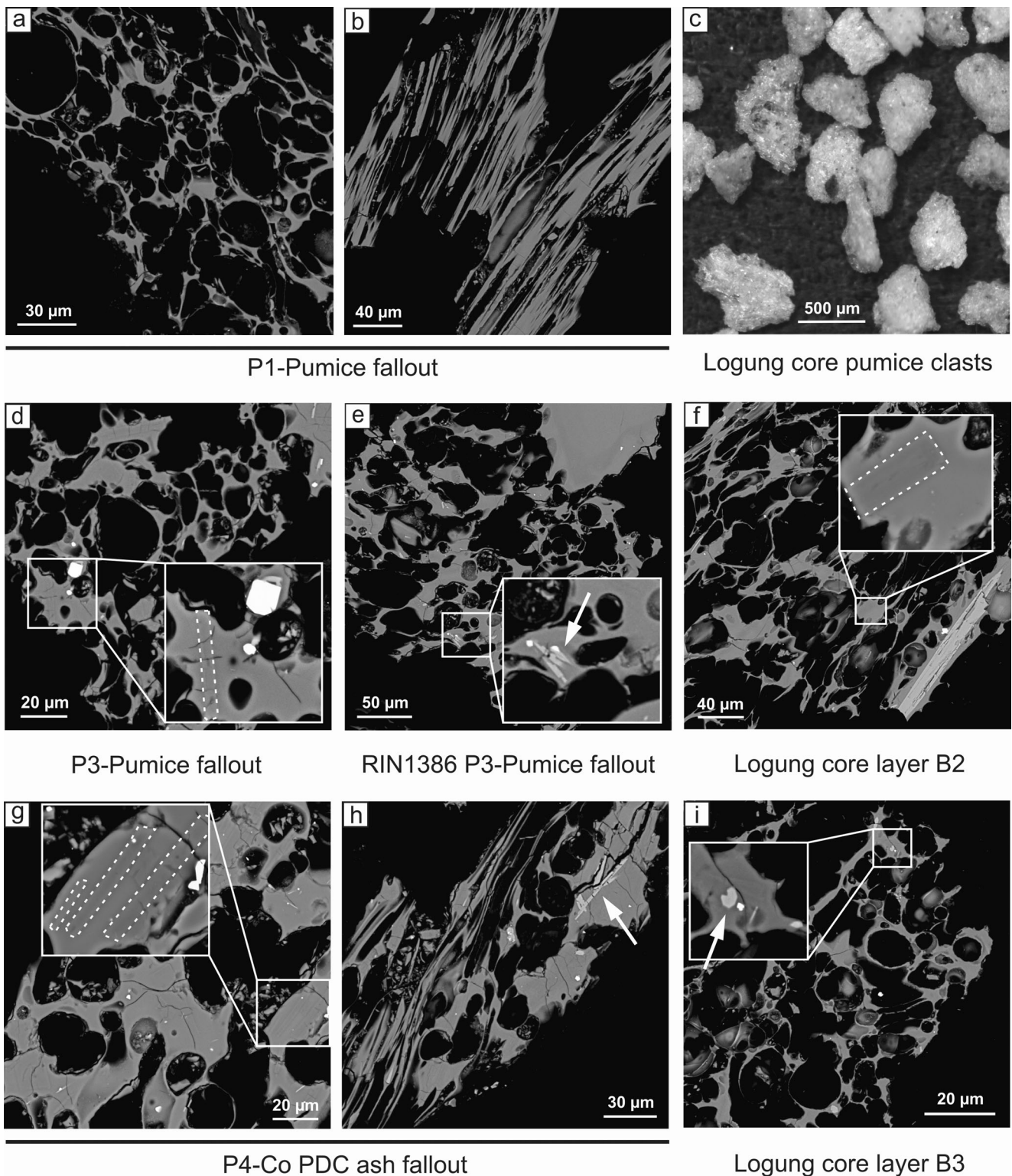


Fig. 5 Backscattered electron microscope images of pumice clasts characteristic of the 1257 A.D. deposits. **a, b** Two representative populations of pumice clasts from P1-PF at locality RIN1392. **c** Binocular image of pumice clasts from Logung core layer B2. **d** Pumice clasts from P3-PF at locality RIN1392. Microlites are

emphasised with *dashed lines* and *arrows*. **e** Suspected pumice clasts from P3-PF at locality RIN1386. **g, h** Pumice clasts from P4-AF at locality RIN1392. **f, i** Pumice clasts from layers B2 and B3 of the Logung core, respectively (see Fig. 3)

several hundreds of kilometres away from source can only originate from the P1 and P3 pumice fallouts and/or the P4-AF co-PDC ash fallout, all of which have the same chemical characteristics. In order to identify which tephra was deposited at Lake Logung, the textures of pumice clasts of both medial (Bali, site RIN1392) and distal deposits were studied using backscattered scanning electron (BSE) imaging (Fig. 5). The pumice clasts from the two distal ash layers of the Logung core were compared to those of the three main fallout units at the medial type section RIN1392 (Figs. 2 and 3b). P1-PF pumice clasts (Fig. 5a) are highly vesiculated and devoid of microlites and occasionally show tubular textures (Fig. 5b). P3-PF pumice clasts (Fig. 5d) strongly differ from the former by the presence of microlites in the matrix glass (feldspar, pyroxene and Fe-Ti oxides), the more fluidal textures, and the virtual absence of fibrous pumice. P4-AF pumice clasts (Fig. 5g, h) show similar textural characteristics than P3-PF clasts, except for the presence of some fibrous microlite-free clasts that originated in phase P1. In the Logung core, pumice clasts (Fig. 5f, i) all contain microlites that attest that none of these layers could originate from P1-PF. No critical textural difference can be observed between the two layers of the Logung core from the BSE images. Thus, we interpret the lowermost layer B2 to correspond to P3-PF and the upper layer B3 to P4-AF. The presence of microlites in the pumice clasts of RIN1386 deposit (Fig. 5e) confirms the widespread dispersal of the P3-PF from the E and SE of Lombok to Sumbawa Island.

No sedimentological criteria can be used to unequivocally correlate the 1257 A.D. Samalas tephra identified at the RIN1401 site on the flanks of Merapi (Figs. 2 and 3d) to one specific pumice fallout units identified in more proximal outcrops. However, the presence of diagnostic microlites in its pumice clasts (Online Resource 3, Fig. S1) confirms that it is a mix of ultra-distal P4-AF and P3-PF.

Spatial distribution of the 1257 A.D. deposits

Isopach maps

Isopach maps of P1-PF, P2-PF and P3-PF are presented in Fig. 6 following the method described in Online Resource 2. The maximum thickness observed for P1-PF deposit is 182 cm at the RIN1307 type locality (Figs. 2, 3a), 23 km SW of the source. The cumulative thickness of pumice fallouts P2-PF1 and P2-PF2 deposited during the phreatomagmatic phase P2 is reported in a single isopach map (Fig. 6b). These fallouts show a plinian dispersal that suggests, together with the nature of the P2 deposits described above, that they resulted from a phreatoplinian phase (Houghton et al. 2000). Isopach maps of the three units of pumice fallouts deposited during phase P3 are represented in Fig. 6c, d based on

cumulative thickness of PF1, PF2 and PF3 units. The recognition of the 2- to 3-cm-thick tephra layer of P3-PF in the Logung core (Fig. 3c) allows us to construct a distal isopach contour line (Fig. 6d). Uncertainties on distal isopach construction are discussed in Online Resource 2. All three maps show ellipsoidal contour patterns indicating strong fallout dispersion towards the W-SW. Indeed, P1-PF and P3-PF are still 17 and 12 cm thick, respectively, on the flanks of Agung (Fig. 2, outcrop RIN1392), 90 km from the source. Isopach maps of P3-PF (Fig. 6c, d) show a wider dispersal upwind and crosswind than P1-PF, with the deposit identified in the Logung core, 340 km downwind. Isopach contours for P4 co-PDC fallout are constructed based on scarce available thickness data due to deposition offshore (Fig. 7). The upper ash layer in the Logung core (Fig. 3c) permitted, however, to construct a 3-cm isopach. Since the primary thickness of the 1257 A.D. Samalas tephra identified at site RIN1401 on the flanks of Merapi could not be measured, a last contour point is extrapolated based on the thinning trend of the deposit, as discussed further. Although the vent location cannot be precisely constrained by the isopach or isopleth maps (see next section) given that very proximal data is missing, it was most likely located where the present-day caldera is.

Isopleth maps

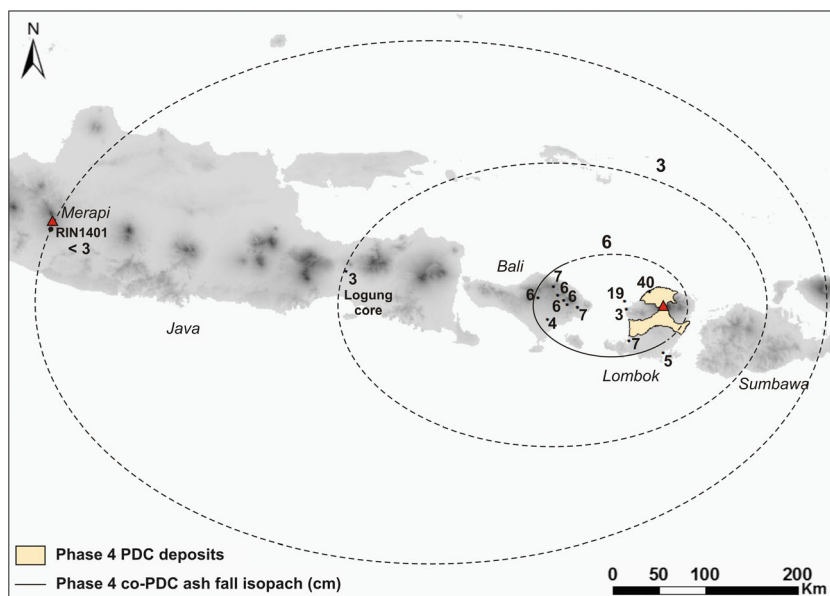
Maximum lithic (ML) and maximum pumice (MP) isopleth maps of P1-PF and P3-PF (Fig. 8) were constructed based on the most reliable values of ML and MP, using the method of Bonadonna et al. (2013) described in Online Resource 2. Although isopleth maps are well constrained for P1-PF (Fig. 8a, b) due to the good preservation of the deposit, isopleth contours of P3-PF (Fig. 8c, d) are constrained by only a few points from localities where the deposit is not eroded by overlying P4-PDC deposits. The greater extension of P3-PF isopleth contours suggests that plume height and mass eruption rate increased during the transition from phase P1 to P3.

Eruptive dynamics

Erupted volumes

The most realistic tephra volume estimation is constrained by the dataset that best describes the thinning trend of a fallout deposit. Empirical data and theoretical modelling of tephra sedimentation from a volcanic plume shows that tephra deposits are characterised by an exponential thinning trend with distance composed of three to four exponential segments that correspond to different sedimentation regimes (Bursik et al. 1992; Bonadonna et al. 1998). Ideally, the thinning trend of a fallout deposit should thus be described by 10–15 isopach contours (Bonadonna et al. 1998; Bonadonna and Houghton

Fig. 7 Onshore distribution of PDCs emplaced during phase P4 and isopach contours of associated P4 co-PDC ash fallout. Thicknesses are given in centimetres. Thickness of the 1257 A.D. Samalas tephra sampled at site RIN1401 on the flanks of Merapi is unknown but likely to be lower than the 3 cm measured in the Logung core, closer to source (see text)



2005). Estimation of the volumes of the different 1257 A.D. fallout units is problematic because of the lack of proximal (0–20 km) and very distal data (>120 km) downwind as well as in crosswind directions, NW and SE of the source. Field data allowed us to constrain eight, five and six isopach contours for P1-PF, P2-PF and P3-PF units, respectively (Fig. 6). In these cases, the deposit thinning for each phase can be approximated by two or three segments on a $\log T$ vs. \sqrt{A} plot, where T is the deposit thickness in metres and A the isopach area in square metres (Pyle 1989, 1995; Fierstein and Nathenson 1992), that yield a minimum volume that is likely underestimated by a factor of 2.5 (Bonadonna and Costa 2012). When three exponential segments are available, the thinning trend of tephra fallouts can be better described by a power-law fit (Bonadonna and Houghton 2005) given by $T = T_{pl}\sqrt{A}^{(-m)}$ where T_{pl} is the power-law coefficient and m the power-law exponent. This method requires the definition of arbitrary proximal and distal integration limits as integration between 0 and infinity is not possible. Bonadonna and Costa (2012, 2013) suggest using a Weibull fit that reproduces the most natural gradual thinning. Tephra volumes are then calculated as a function of the characteristic decay length scale of deposit thinning λ_{th} by the relation $\text{Volume} = 3.10^6 \times \lambda_{th}^{1.53}$. These three methods were used to calculate the tephra volumes associated with the P1, P2 and P3 phases of the 1257 A.D. Samalas eruption. Their associated thinning trends are represented in Fig. 9. Values were computed using AshCalc software (Daggit et al. 2014). Erupted volumes, masses and corresponding magnitudes calculated for each phase are given in Table 2.

Integration of a three-segment exponential fit for P1-PF (Fig. 9a) yields a volume of 5.8 km³ (Table 2), which is

considered as a minimum value since distal data is missing (Pyle 1995). The power-law fit yields a similar volume of 5.4 km³ (with 16 and 1500 km chosen as proximal and distal limits, respectively). The Weibull fit yields a higher bulk volume of 12.3 km³ based on eight isopach contours and 13.4 km³ by eliminating the last 4-cm isopach. Given that the latter is poorly constrained (1 point) and its shape is based on the method of ellipses (Sulpizio 2005), its area is likely underestimated. The most realistic bulk volume (Bonadonna and Costa 2013) should thus be within a range of 12.6–13.4 km³, which corresponds to a dense rock equivalent volume of 3.0–3.3 km³ (rock density 2470 kg/m³; deposit density 603 kg/m³). The associated erupted mass for P1 is 7.4–8.1 × 10¹² kg, which corresponds to a magnitude of 6 (Table 2).

Pumiceous tephra produced during the phreatomagmatic phase P2 (P2-PF1 and P2-PF2) have a minimum bulk volume of 0.9 km³ based on the two-segment exponential thinning trend and 3.5 km³ according to the Weibull fit integration (Fig. 9b). Considering that only five isopach contours were constructed for this deposit (Fig. 6b), we did not use the power-law method and considered that the Weibull method should give a more reliable maximum volume value. Hence, a best estimate of the bulk volume of the P2 pumice fallout is 0.9–3.5 km³, which corresponds to 0.3–1 km³ DRE (rock density 2470 kg/m³; deposit density 714 kg/m³), an erupted mass of 0.7–2.5 × 10¹² kg and a magnitude of 5 (Table 2). A minimum estimate of the amount of external water that interacted with the magma during phase P2 can be approximated from the minimum water/magma ratio of 0.3 required to explain the observed deposit textures, i.e. wet dilute turbulent PDC deposits (surges) and abundant accretionary lapilli (Sheridan and Wohletz 1983). A magma volume of 0.3–1 km³ DRE yields a water volume of 0.1–0.3 km³ that likely

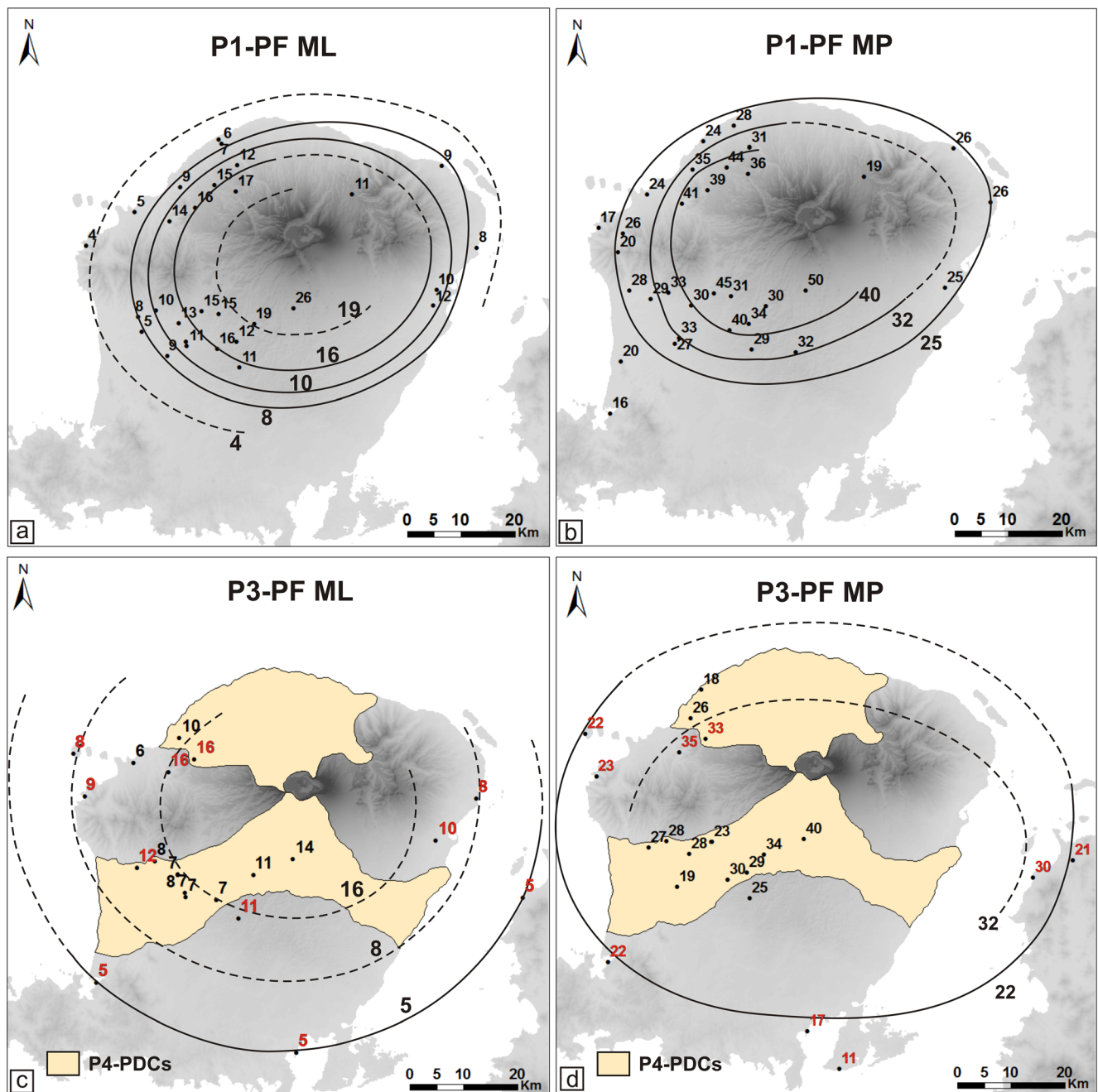


Fig. 8 **a, b** Maximum lithic (ML) and maximum pumice (MP) isopleths maps of P1-PF, respectively. **c, d** ML and MP isopleths maps of P3-PF, respectively. Extent of phase 4 PDC deposits is shown. Reported numbers represent the geometric mean of the three axes of the 50th percentile of

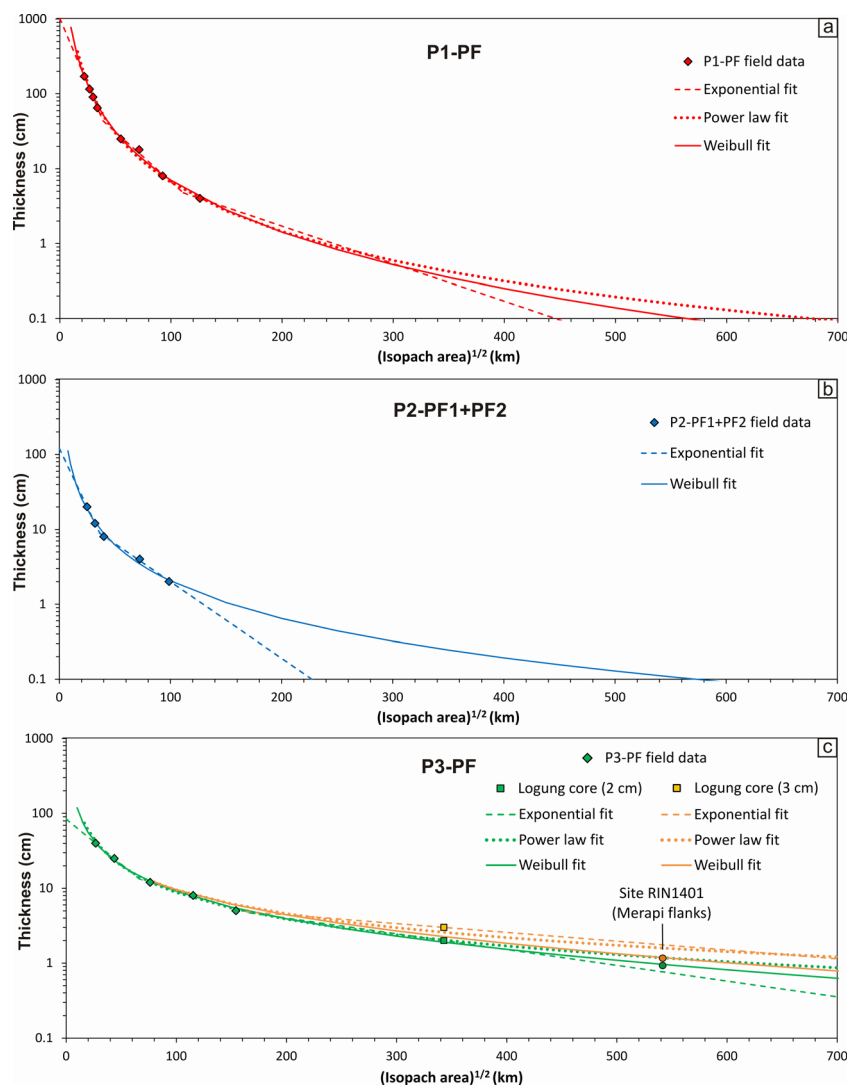
the 20 largest clasts, given in millimetres. *Red numbers* are the most reliable values (i.e. where P3-PF deposits not eroded by P4-PDCs) considered for constructing the isopleth contours

originated from either the perched aquifers within the upper parts of the edifice or a pre-eruption crater lake.

A minimum bulk volume of the P3 pumice fallout was first estimated based on the five proximal isopach contours (Fig. 6c), without taking into account the most distal point in the lake Logung core. Integration of the two-segment exponential fit and of the Weibull fit yields bulk volumes of 5.0 and

8.1 km³, respectively (Table 2). Figure 9c shows the thinning trends obtained with the three methods when incorporating the last isopach contour, for thickness values of 2 and 3 cm in the Logung core. The curves show that both power-law and Weibull thinning trends do not fit the last data point well using a value of 3 cm, given that the Weibull fit indicates a value of 2.3 cm for the last contour point. The Weibull approximation

Fig. 9 a–c Log T vs. \sqrt{A} plot of P1-PF, P2-PF1+PF2 and P3-PF deposits. Thinning trends are approximated by exponential, power-law and Weibull fits. Two choices for fitting distal part of thinning trend are inferred for P3-PF based on the thicknesses of 2 and 3 cm of tephra in the Logung core. *Circles* indicate extrapolated thickness of P3-PF deposit at site RIN1401 on the flanks of Merapi, based on two Weibull fits



fits better with a value of 2 cm (Fig. 9c). This result strongly suggests that the primary thickness of P3-PF in Lake Logung is most likely 2–2.3 cm. This distal point is critical since it increases the bulk volume determined by using only proximal isopachs by a factor of ca. 2. Integration of the three-segment exponential fit, the power-law fit (with 16 and 1500 km chosen as the proximal and distal limits, respectively) and the Weibull fit yield volumes of 10.2, 13.5 and 18.8 km³, respectively, using a value of 2 cm for the most distal isopach (Table 2). Given that the Weibull fit describes better the process of very distal thinning than the exponential and power-law approximations (Bonadonna and Costa 2013), we estimate that the bulk volume of P3-PF deposit is 18.8–21.7 km³, based on a distal isopach of 2 to 3 cm. The corresponding DRE volume is 4.1–4.7 km³ (rock density 2470 kg/m³; deposit density of 539 kg/m³). Moreover, since most proximal points do not represent the full thickness of the deposit due to erosion, this value should be considered as a minimum volume range for P3-PF. Phase 3 thus erupted 1.0–1.2 × 10¹³ kg of material, more than phase 1, with

a peak magnitude of 6 (Table 2). Considering that the 1257 A.D. Samalas tephra identified at the outcrop RIN1401 on the flanks of Merapi corresponds to a \sqrt{A} value of ca. 550 km from the source based on the eccentricity of the more proximal contours (Sulpizio 2005), we can extrapolate from the Weibull fits an expected thickness range of 0.9–1.2 cm for distal P3-PF tephra at site RIN1401, located 660 km downwind from source (Fig. 9c). Hence, we confirm that the minimum observed thickness for the 1257 A.D. Samalas distal tephra units in the Merapi area ranging from 1 to 2.5 cm represents a cumulative minimum thickness for P3-PF and P4-AF units. Pumice fallout produced by phases 1, 2 and 3 together represent a cumulative bulk volume of 32–39 km³ and a DRE volume of 7–9 km³.

New field observations on the distribution of the onshore PDCs emplaced during phase P4 allow us to estimate depositional areas of 554 and 878 km² for the northern and southern P4-PDC units (Fig. 7), respectively. The P4-PDC deposits are, on average, 18 m thick (measured at 10 locations) at the N of

Table 2 Determination of the volume, mass and magnitude of fallout units for each eruptive phase of the 1257 A.D. Samalas eruption using different methods

Eruptive phase	Method	Bulk volume (km ³)	DRE volume (km ³)	Erupted mass (kg)	Magnitude ^a
P1-PF	3 segments, exponential fit ^b	5.8			
	Power-law fit ^c	5.4			
	Weibull fit ^d	12.3–13.4	3.0–3.3	7.4–8.1×10 ¹²	6
P2-PF1+PF2	2 segments, exponential fit ^b	0.9	0.3	0.7×10 ¹²	5
	Weibull fit ^d	3.5	1.0	2.5×10 ¹²	
P3-PF	No distal point				
	2 segments, exponential fit ^b	5.0			
	Weibull fit ^d	8.1			
Including Logung point	3 segments, exponential fit ^b (Logung 2 cm)	10.2			
	Power-law fit ^c (Logung 2 cm)	13.5			
	Weibull fit ^d (Logung 2–3 cm)	18.8–21.7	4.1–4.7	1.0–1.2×10 ¹³	6
P4-AF	One segment exponential fit ^b	20–24	8–9	1.9–2.2×10 ¹³	6

DRE dense rock equivalent

^a Pyle (2000), $M = \log_{10}(\text{erupted mass}) - 7$

^b Fierstein and Nathenson (1992), Pyle (1989, 1995)

^c Bonadonna and Houghton (2005)

^d Bonadonna and Costa (2013)

Lombok, whereas SW and SE, they average about 23 m in thickness (measured at eight locations). We thus approximate a bulk volume of 29 km³, equivalent to a minimum DRE volume of 16 km³ (rock density 2470 kg/m³; deposit density 1370 kg/m³, Lavigne et al. 2013). The volume of offshore PDC deposits remains unknown. Hence, the uncertainty on the total volume of PDCs produced during the 1257 A.D. eruption is large. Ongoing investigation on the reconstruction of the pre-1257 topography of Lombok will provide better constraints on the volume of PDCs.

The two isopach contours for P4 co-PDC ash fallout (Fig. 7) are insufficient to properly describe the thinning trend of the deposit. Based on the assumption that some of the co-PDC ash produced by the elutriation from P4-PDCs could have fed the collapsing column and been deposited at large distances (Sparks and Walker 1977), we consider that very distal fine ash (i.e. >340 km from the source) from both P3-PF and P4-AF would have sedimented in a similar regime at Lake Logung (East Java) and at the RIN1401 site on the flanks of Merapi. Hence, we apply the same thinning trend of P3-PF from the Logung core to the site RIN1401 (2–2.3 cm down to 0.9–1.2 cm) to the P4-AF deposit. A thickness of 3 cm of P4-AF in the Logung core thus suggests a deposition of ca. 1.5 cm of P4-AF at site RIN1401. This value is *hypothetical* but its determination is fundamental to roughly quantify the volume of the P4-AF deposit. However, it is conceivable that at such distances, ash from both phases 3 and 4 has mixed, forming a single tephra layer in which P4-AF is more abundant. An isopach contour is assigned to this point based on the eccentricity of the 3- and

6-cm contours (Sulpizio 2005). With three isopach values, the integration of a single exponential segment is the only method applicable. It yields a minimum bulk volume of 20–24 km³ (Table 2), equivalent to 8–9 km³ DRE (rock density 2470 kg/m³; deposit density 914 kg/m³). Taking into account the volume of onshore PDC deposits, phase 4 thus erupted a minimum DRE volume of ca. 25 km³, 3 times the cumulative volume erupted by P1, P2 and P3 phases.

Column height and wind speed

The eruptive column height H_T was derived with the method of Carey and Sparks (1986) with ML isopleths for both P1-PF and P3-PF (Fig. 8a, c). MP isopleths were not used to calculate H_T since the densities of both P1-PF and P3-PF pumice clasts do not match (400 and 600 kg/m³, respectively, Online Resource 2) with those that can be used with the model of Carey and Sparks (1986). Furthermore, the use of ML isopleths is generally preferred when data is available because the greater tendency of pumice clasts to break upon impact with the ground results in greater uncertainties on the MP values. Recently, Bonadonna and Costa (2013) introduced a new method to estimate the maximum H_T by using a Weibull parameter λ_{ML} , that is derived from the relation between ML and the square root of the isopleth area and that allows to determine the H_T by the empirical relationship $H_T = 5.01 \times \lambda_{ML}^{0.55}$. ML isopleths of both 16 and 8 mm for P1-PF yield a H_T of 39 km and a wind speed of 10 m/s (Table 3) using the method of Carey and Sparks (1986), whereas the Weibull parameter yields a consistent

Table 3 Determination of the total column height, wind speed, mass discharge rate, duration and intensity for phases 1 and 3 of the 1257 A.D. Samalas eruption using different methods

Phase	Method	H_T (km)	Wind speed (m/s)	MDR ^a (kg/s)	Duration (h)	Intensity ^b
P1-PF	CS86 ^c ML 8 mm	39	10	2.8×10^8	6–8	11–12
	CS86 ^c ML 16 mm	39	10			
	Weibull ^d	40		3.6×10^8		
P3-PF	CS86 ^c ML 8 mm	43	12	4.6×10^8	6–7	12
	CS86 ^c ML 16 mm	38	12	2.8×10^8		
	Weibull ^d	59				

ML maximum lithic (accidental) size, H_T eruption column height, *MDR* mass discharge rate

^a Estimated with the method of Carazzo et al. (2008)

^b Pyle (2000), $I = \log_{10}(\text{MDR}) + 3$

^c Carey and Sparks (1986)

^d Bonadonna and Costa (2013)

H_T of 40 km. Hence, the eruptive plume of P1 reached a total height of 39–40 km.

The method of Carey and Sparks (1986) yields a range of H_T of 38–43 km with a wind speed of 12 m/s for P3-PF, based on the 8- and 16-mm isopleths (Table 3). Discrepancies between H_T values are associated with the lack of reliable data for this pumice fallout deposit consisting of three distinct fallout units that grade into each other, as well as with the uncertainty on the shape of the 16-mm isopleth contour (Fig. 8c), given that proximal ML values are less well constrained (erosion processes). Furthermore, field evidence of a wider of H_T with the Weibull method yields an unrealistic value of 59 km (Table 3), due to the lack of isopleth contours and possibly due to an underestimation of the area of the 16-mm isopleth, that in turn generates an overestimation of λ_{ML} . As a result, a maximum value of 43 km is considered to be the most realistic H_T for P3-PF.

Mass discharge rate and duration

The mass discharge rate (MDR) is inferred from the maximum plume height by using the model of Carazzo et al. (2008) with the magmatic conditions of the 1257 A.D. eruption. The MDR was calculated for each value of H_T (Table 3) under tropical atmosphere conditions, considering a magma temperature of 1000 °C determined by homogenisation of melt inclusions in plagioclase and a dissolved water content of 5 wt% as derived from preliminary FT-IR spectroscopy data (Vidal et al. 2013). The estimated values of H_T for P1-PF yield a range of MDR of $2.8\text{--}3.6 \times 10^8$ kg/s, which corresponds to a duration of 6–8 h and an intensity of 11–12 (Pyle 2000). H_T value of P3-PF yields a maximum MDR of 4.6×10^8 kg/s corresponding to a duration of 6–7 h. Hence, P3 is the most explosive phase of the 1257 A.D. eruption. Considering the duration of the two plinian phases P1 and P3, and without taking into account phase P2, the eruption lasted a minimum of 12–15 h, given that there is no stratigraphic evidence of a remarkable hiatus from P1 to P3.

Discussion

Total erupted volume

The estimation of the volume of tephra fallout is based on determining the thinning trend of a deposit with distance from the source, to which different mathematical functions can be fitted (Pyle 1989, 1995; Fierstein and Nathenson 1992; Bonadonna and Houghton 2005; Bonadonna and Costa 2013). The accuracy of each of these methods strongly relies on the dataset available and its spatial distribution (Engwell et al. 2013), as the sedimentation regime of tephra varies with distance from the source (Bonadonna et al. 1998). Acquisition of very distal data allowed us to determine the volume of pumiceous tephra produced by each phase more accurately. The total bulk volume of P1, P2 and P3 pumice fallouts reaches a *minimum* of 7–9 km³ DRE, twice the DRE volume (3.7–4.8 km³) estimated by Lavigne et al. (2013). Moreover, half of this volume is associated with the P3 pumice fallout, contrary to previous estimates that suggested that P1 was the most intense phase of the eruption. New constraints on P4-PDC deposits inland allow us to determine a DRE volume of 16 km³, twice the previous volume estimated (8 km³) by Lavigne et al. (2013). Scarce data for P4 co-PDC ash fallout yield a minimum volume of 8–9 km³ DRE that is very likely an underestimate, but equivalent to the DRE volume of P1, P2 and P3 pumice fallouts. The total DRE volume of ca. 33 km³ (31–34 km³) calculated from mapped deposits is thus a *minimum* erupted volume.

Lavigne et al. (2013) estimated a total DRE volume of 40 ± 3 km³ through the reconstruction of pre-caldera topography by summing (i) the volume of the current caldera and the missing upper Samalas edifice, (ii) the volume of the debris avalanche from the collapse of the western flank of the Rinjani edifice entirely into the caldera and (iii) the volume of the Barujari post-caldera products. However, the possible existence of a crater lake prior to the 1257 A.D. eruption, evidenced by widespread phreatomagmatic deposits and our preliminary estimate of the water/magma ratio associated with phase P2, suggests

that the pre-caldera topography of Mt Samalas is more complex than the model of Lavigne et al. (2013). The minimum volume of water involved (0.1–0.3 km³), however, is well within the error margin (± 3 km³) of the total erupted volume estimate. Furthermore, this volume calculation does not take into account the unknown volume of pyroclastic material that might have fallen into the caldera during or after the eruption and which would underestimate the volume of the caldera. Indeed, the internal structure of the caldera and the geometry of the caldera fill are totally unknown. We thus consider a well-constrained total DRE volume range of 33–40 km³, corresponding to a total magnitude of 7. However, it is likely that future studies will arrive at a volume estimate that could exceed 40 km³ by a few cubic kilometres.

The volume of offshore PDCs and of the magma involved in phase P2 can be estimated from the difference of the caldera volume (40 ± 3 km³ DRE) and the total DRE volume from mapped deposits of P1-PF, P2-PF, P3-PF, onshore P4-PDC and P4-AF. The missing volume is ~ 7 km³ DRE, which partly includes the unmapped P4 co-PDC ash fallout. The assessment of the P4-AF volume is the most complex because of its widespread regional deposition, largely offshore. It is however the most fundamental since it can represent most of the erupted volume (e.g. 1815 Tambora eruption: Self et al. 1984, 2004; Sigurdsson and Carey 1989; Kandlbauer and Sparks 2014; 7630 B.P. Mazama eruption: Young 1990). Our ongoing detailed investigation of marine cores in the Bali Sea North of Lombok and in the Indian Ocean South of Lombok (collaboration with W. Kuhnt; Vidal et al. 2015) will provide additional constraints on the ultra-distal fallout deposits, especially the P4-co-PDC fallout.

Classification of the 1257 A.D. Samalas eruption

Several classification schemes for volcanic eruptions have been proposed based on plume height, fragmentation and dispersal indexes (Walker 1973; Pyle 1989) or eruption magnitude and intensity (Newhall and Self 1982; Pyle 2000). The magnitude 6 estimated for the P1 pumice fallout is equivalent to a VEI 6 eruption (Newhall and Self 1982; Crosweller et al. 2012) and would correspond to a strong plinian eruption. Based on the three-segment extrapolation on the $\log T$ vs. \sqrt{A} plot for P1-PF (Fig. 9a), a near-vent deposit thickness T_{\max} of 10.2 m is inferred. This value yields a dispersal index D of 7500 km², based on the area enclosed within the 0.01 T_{\max} as defined by Walker (1973). Considering an H_T of 39–40 km for P1-PF, this phase clearly plots within the plinian field defined by Pyle (1989). Bonadonna and Costa (2013) established a new classification scheme based on the Weibull decay parameters of ML and thickness with distance from source (λ_{ML} and λ_{th}) assuming a typical uncertainty of 20 % for plume height. This classification is presented

in Fig. 10 integrating new values for both P1 and P3 pumice fallouts of the 1257 A.D. Samalas eruption. According to this scheme, P1-PF plots on the plinian/ultraplinian border and could thus be considered as transitional plinian-ultraplinian.

The magnitude 6 of P3 pumice fallout is equivalent to a VEI 6 eruption (Newhall and Self 1982; Crosweller et al. 2012). A near-vent T_{\max} of 84 cm is obtained by extrapolation of the exponential fit plot (Fig. 9c), a minimum value since the proximal thinning observed is truncated due to erosion of the deposit. This value yields a maximum dispersal index D of 110,500 km² (Walker 1973) that would classify the P3-PF as ultraplinian (Pyle 1989). In the classification scheme of Bonadonna and Costa (2013), P3 pumice fallout plots within the upper 20 % plinian-ultraplinian boundary (Fig. 10). Since the Weibull approximation of H_T is not reliable for our three-isopleths dataset, the λ_{ML} parameter was estimated for the H_T value of 43 km derived from the model of Carey and Sparks (1986). Considering a typical uncertainty of 20 % on plume height, this event is classified as transitional plinian-ultraplinian, ranking among the most powerful Holocene explosive eruptions (Fig. 10). The very distal data point of P3-PF in the Logung core and the lack of data between the last two points cause a shift in the λ_{th} parameter that approaches its upper limit of 1000 km.

Comparisons between eruptions based on this new classification scheme (Fig. 10) should be made carefully since H_T values are estimated with different ML calculation methods. In particular, plume heights (and thus λ_{ML}) estimated on the basis of the average of the geometric mean of the three axis of 5 and 3 largest clasts are likely to be overestimated, depending on the sampling method. Our results showed that the choice of the 50th percentile of the 20 largest clasts yielded stable values of H_T for P1 pumice fallout for both 8- and 16-mm isopleth contours with the method of Carey and Sparks (1986). Bonadonna and Costa (2013) suggested a more reliable classification scheme based on the decrease of the Inman parameter $Md\phi$ with distance from the vent, which can also be described by a Weibull function by plotting λ_{th} vs. $\lambda_{Md\phi}/\lambda_{th}$ and would be more accurate than the decrease of the ML size.

The absence of any known eruption that would plot above the upper 20 % boundary of plinian-ultraplinian of this classification (i.e. with a plume height >49 km) casts doubts on the existence of the ultraplinian field as defined by Bonadonna and Costa (2013). Furthermore, recent re-analysis of the re-dated (Sigl et al. 2013) 232 A.D. Taupo deposit (Houghton et al. 2014), the only known ultraplinian eruption so far, showed that the extremely widespread dispersal estimated by Walker (1980) was biased by a shift in wind direction resulting in the expansion of isopachs and isopleths fields. Houghton et al. (2014) concluded that the Taupo eruption was of plinian intensity. These results suggest that the upper limit of a plume height is unlikely to exceed ~ 45 km. Hence,

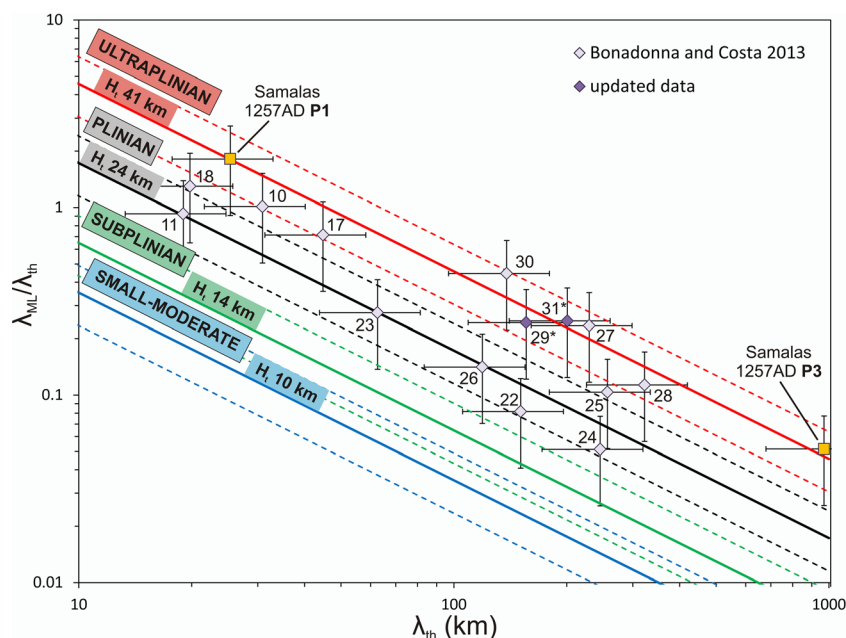


Fig. 10 Eruption classification scheme modified from Bonadonna and Costa (2013, Fig. 6) using the correlation of λ_{th} vs. $\lambda_{ML}/\lambda_{th}$. Red, black and green solid lines represent theoretical lines for H_T of 41, 24 and 14 km, respectively, based on the correlation of Eq. 7 of Bonadonna and Costa (2013) (H_T of 10 km is also shown as a blue solid line for reference). Dashed lines represent 20 % error on H_T values. Diamonds represent data of Bonadonna and Costa (2013). Dark-purple diamond #29* is the 232 A.D. Taupo eruption with an updated value for λ_{ML} based on new estimates of H_T (35–40 km; Houghton et al. 2014). Diamond

#31* is the 1815 Tambora eruption with a λ_{th} value calculated based on pumice fallout volume (10 km³ DRE; Kandlbauer and Sparks 2014). Yellow squares are data for the 1257 A.D. Samalas P1 and P3 phases. Error bars of 30 and 50 % are also shown, associated with λ_{th} and $\lambda_{ML}/\lambda_{th}$, respectively. Labelled symbols of Bonadonna and Costa (2013): El Chichon A (#10), Fogo A (#11), 232 A.D. Hatepe (#17), 1886 Tarawera (#18), 1912 Novarupta A, C and F (#22, #23, #24, respectively), 1932 Quizapu (#25), 1902 Santa Maria (#26), 1991 Pinatubo (#27), 3600 B.P. Minoan (#28) and 3500 B.P. Waimihia (#30)

the upper 20 % plinian-ultraplinian boundary as defined in Fig. 10 should be considered as an upper limit, and the definition of the ultraplinian field should be reconsidered.

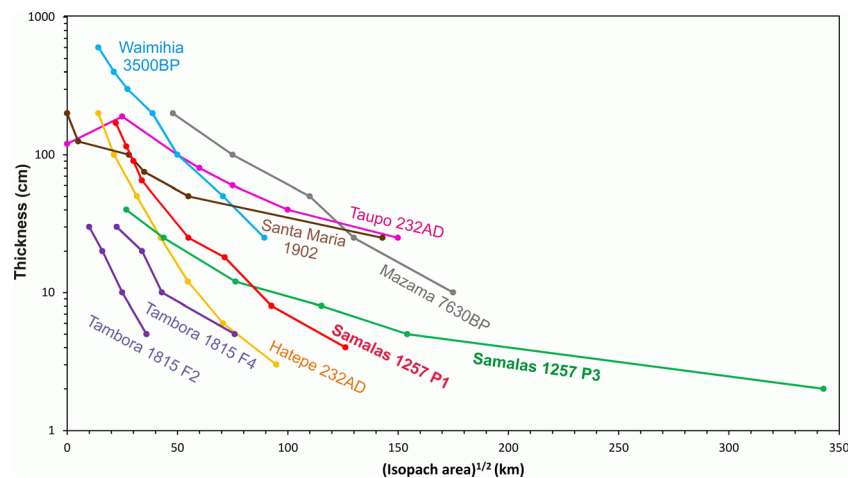
Figure 11 compares the 1257 A.D. Samalas P1 and P3 pumice fallout thinning trends to those of pumice fallout deposits from explosive eruptions of similar intensity. For all of these eruptions, the lack of distal thickness data (i.e. the last segment corresponding to the sedimentation of very fine ash; Bonadonna et al. 1998) likely underestimates the dispersal. The classification based on the dispersal index D for large explosive eruptions thus strongly relies on the availability of very distal data. Among those eruptions, the P3-PF deposit of the 1257 A.D. eruption has the greatest extent along the dispersal axis because it has been identified at least as far as 340 km from the source. Hence, the P3 deposit is associated with one of the largest dispersals ever documented. No evidence of a shift in wind direction was found for P3-PF but cannot be excluded however, given that the three sub-units of the P3-PF deposit were only observed together at three localities downwind. The 1815 Tambora eruption was of the same order of magnitude (41 ± 4 km³ DRE) and intensity (MDR of 2×10^9 kg/s), with a maximum column height of 43 km (Self et al. 1984, 2004; Sigurdsson and Carey 1989; Kandlbauer and Sparks 2014). However, its pumice fallouts F2 and F4 contribute for a small part to the total volume and dispersal,

most of which is represented by the F5 co-ignimbrite ash fallout. The thinning trends for F2 and F4 reported in Fig. 11 yielded a total plinian fallout volume of 1.8 km³ DRE (Sigurdsson and Carey 1989). Kandlbauer and Sparks (2014) re-estimated the volume of the climactic plinian phase to 10 km³ DRE based on the duration and the new mass eruption rate inferred from the model of Woods and Wohletz (1991). Hence, this new volume is comparable to the 7–9 km³ DRE volume calculated for the plinian fallouts of the 1257 A.D. eruption, even though the P1 and P3 pumice fallout thinning trends plot well above those of the 1815 Tambora fallouts in Fig. 11.

The phreatomagmatic phase P2 is complex and requires the analysis of detailed grain size and textural data that is beyond the scope of this paper. Nevertheless, the variety of features observed in P2 deposits such as thick widespread accretionary lapilli-bearing units, very fine ash fallout and far-reaching mobile wet dilute PDCs, together with the plinian dispersal of associated pumice units, is compatible with a phreatoplinian eruptive style in its broadest definition (Houghton et al. 2000).

The maximum MDR of 4.6×10^8 kg/s estimated for the 1257 A.D. eruption with the model of Carazzo et al. (2008) is in agreement with an MDR of 5×10^8 kg/s required to maintain a stable plume under tropical atmospheric conditions with

Fig. 11 Log T vs. \sqrt{A} plot of 1257 A.D. Samalás P1 and P3 pumice fallout deposits compared with the thinning trends of pumice fallout deposits from other large plinian eruptions. References: Waimihia and Hatepe (Walker 1981); Mazama (total pumice fallout; Young 1990); Taupo (Walker, 1980); Santa Maria (Williams and Self 1983); Tambora F2 and F4 (Sigurdsson and Carey 1989)



a magmatic temperature of 1000 °C (Sparks 1986). Our results show that this critical limit was reached during the phase P3, and the model of Carazzo et al. (2008) suggests that a maximum flux of 1×10^9 kg/s would have been necessary to provoke the wholesale column collapse. This suggests that the collapse and the emplacement of voluminous pyroclastic density currents and associated co-PDC ash fallout during phase P4 are likely the result of the formation of a large caldera.

With a total erupted volume of 33–40 km³ DRE, an overall magnitude of 7 and a climax intensity of 12 (Tables 2 and 3), the 1257 A.D. eruption of Samalás constitutes a remarkable case study of a historic major plinian eruption with well-preserved proximal and ultra-distal deposits. It is one of the most violent volcanic events of the last 2000 years, together with the 1815 Tambora and the 232 A.D. Taupo eruptions. However, the uniqueness of this eruption remains its extremely high SO₂ release estimated at 170 Mt, significantly higher than the 100 and 45 Mt released during the 1458 A.D. Kuwae (30–60 km³ DRE; Witter and Self 2007) and 1815 Tambora eruptions, respectively (Sigl et al. 2014). Even though the eruptive parameters are poorly constrained for the Kuwae eruption, these three caldera eruptions have similar magnitudes and intensities. The exceptional SO₂ release might be explained by a better transport of particles into the stratosphere during the 1257 A.D. eruption of Samalás as a result of a continuous ash injection without significant hiatus from the P1 to the P4 phase during a minimum of 12–15 h. In contrast, the two plinian events F2 and F4 of the 1815 Tambora eruption occurred over a period of 5 days (Self et al. 2004; Sigurdsson and Carey 1989). Furthermore, the P1 phase of the 1257 A.D. Samalás eruption was of stronger intensity (H_T of 39–40 km, MDR of $2.8\text{--}3.6 \times 10^8$ kg/s) than the F2 phase of Tambora (H_T of 33 km, MDR of 1.1×10^8 kg/s; Sigurdsson and Carey 1989). The P3 phase of the Samalás eruption and the F4 phase of Tambora eruption have the same maximum plume height (43 km); however, the estimated MDR of 4.6×10^8 kg/s for P3 is lower than the MDR of $2 \times$

10^9 kg/s for F4. These results suggest that the injection and transport of SO₂ into the stratosphere would have been more efficient in the case of the 1257 A.D. eruption because of the high mass flux reached during the plinian phase P1. Other contributing factors would be a larger volume of erupted magma and/or a better extraction of the sulphur during the genesis and eruption of the magma that led to the 1257 A.D. eruption of Samalás.

Conclusion

The recently discovered 1257 A.D. eruption of Samalás was the subject of a multidisciplinary overall study by Lavigne et al. (2013) who coupled volcanological and geographical data with the exegesis of historical written documents to establish for the first time a direct link with the 1259 A.D. sulphate spikes in polar ice cores. In this work, we present a much more detailed analysis of the deposits of this exceptional eruption constrained by new extensive field work on the islands of Lombok, Sumbawa, Bali and Java, supported by physical, textural and geochemical datasets. Combined to the application of the most recent empirical physical models, this analysis allows us to significantly revise the stratigraphic reconstruction and quantification of the eruptive parameters of the most important eruption of the past millennium, one of the largest of the Holocene.

The eruption is characterised by four phases: (i) an initial plinian phase P1 that produced over 6 to 8 h a widespread pumice fallout of 3.0–3.3 km³ DRE from a 39- to 40-km stable column with a peak MDR of $2.8\text{--}3.6 \times 10^8$ kg/s; (ii) a phreatomagmatic phase P2 that involved a large amount of water that probably originated from a lake and produced widespread turbulent mobile pyroclastic flows, thick accretionary lapilli-rich fine ash fallouts and 0.3–1 km³ DRE of pumice fallout; (iii) a stronger plinian phase P3 that produced over 6 to 7 h a 4.1–4.7-km³ DRE of pumice fallout from an unstable

column that culminated at 43 km with a peak mass eruption rate of 4.6×10^8 kg/s; and (iv) a phase P4 during which the eruption produced sustained low fountaining that climaxed with the formation of a 6.5×8 -km-wide caldera and wholesale column collapse, generating at least ca. 16 km^3 DRE of non-welded pumice-rich pyroclastic density currents that entered the sea producing $8\text{--}9 \text{ km}^3$ DRE of co-PDC ash fall deposited in the surrounding islands and identified as far as 660 km from the source on the flanks of Merapi volcano in Central Java.

The reproducibility of ICP-MS trace element analysis of 3–5 mg of carefully selected pumice clasts yields a strong geochemical correlation of the 1257 A.D. products over 660 km from the source with relative standard deviation of 2–7 %. Hence, this methodology is a valuable tool for tephrochronological studies and a potential alternative to trace element fingerprinting of glass particles by laser ablation ICP-MS. We demonstrate that the 1257 A.D. Samalas eruption constitutes an important inter-regional chronostratigraphic marker since its distal fine-grained ash units have been preserved in various sedimentary environments. This bears important implications for archaeological and historical studies as well as for paleoclimatic and paleoenvironmental research in Indonesia and neighbouring regions of South-East Asia (e.g. Indo-Pacific warm pool).

The collection of very distal data, 660 km downwind from source, was crucial to constrain the thinning characteristics and hence the dispersal of the P3 pumice fallout and P4 co-PDC ash fallout. The P3 pumice fallout is one the most widely dispersed plinian tephra deposit ever documented, with a dispersal index of $110,500 \text{ km}^2$. The very large release of 170 Mt of SO_2 estimated for this eruption (Sigl et al. 2014) can be explained by (i) the efficient transport of gas and particles favoured by the continuous injection from P1 to P4 of finely fragmented tephra at heights ranging from 38 to 43 km and mass discharge rates of up to 4.6×10^8 kg/s and (ii) by a greater volume of magma and/or a better extraction of the sulphur from this magma to the stratosphere. These processes likely contributed to the efficient dispersal and longevity of sulphur-rich aerosols to polar regions and their probable regional and global impact on human communities during the Middle Ages.

With a total magnitude of 7 and a peak intensity of 12, the 1257 A.D. eruption of Samalas ranks among the most powerful events of the last 2000 years. It is especially remarkable that the two most recent and most powerful eruptions in Indonesia, the 1257 Samalas and 1815 Tambora events, have occurred in only a small sector of the volcanic arc (within less than 200 km from each other) in a short time interval of ca. 600 years. This has implications for the potential discovery of additional unknown recent caldera-forming eruptions and the revision of magnitude-frequency distributions for large explosive events in the area and worldwide. Given the evidence of unrest at several calderas in the world (e.g. Santorini, Campi Flegrei, Rabaul, Yellowstone; Newhall and Dzurisin 1989)

and the active status of the Samalas-Rinjani caldera (one the largest thermal anomalies and CO_2 flux measured in a caldera lake; Barbier 2010), improving our understanding of the dynamics and the temporal occurrence of major plinian climate-impacting events such as the Samalas 1257 A.D. eruption is fundamental to enhance our capacity to detect potential pre-eruption unrest and mitigate volcanic risks of active caldera systems at a local and global scale.

Acknowledgments We are grateful to RISTEK for allowing us to undertake this research and the Nusa Tenggara Barat Governor's Office for administrative support. We thank Dr Hendrasto (PVMBG/CVGHM) for his steadfast support and our Indonesian colleagues for field and administrative assistance. We are very grateful to J.-P. Toutain and Etny at IRD for valuable assistance and the institutional support. We are most indebted to Sofie and her staff at PVMBG for their help with administrative procedures and to Didik for the skilful dedicated driving. We also thank F. Le Cornec for her assistance for ICP-MS measurements, S. Hidalgo for pumice density measurements, M. Abrams (NASA) for providing ASTER satellite data and Arlyn (Rinjani Observatory, PVMBG) and H. Rachmat for samples of Barujari lavas. We thank Y. Wahyudi (PVMBG) and participants of the Rinjani excursion (CoV 8) for sharing their ideas. We are grateful for discussions and field insights on Merapi stratigraphy with S. Andreastuti, R. Gertisser and S. Charbonnier, and on marine cores with W. Kuhnt. ^{14}C dates were obtained by C. Moreau and J.-P. Dumoulin (LMC14, CNRS UMS2572). We are grateful to S. Self (editor) and T. Druitt and R. Gertisser (reviewers) for their insightful and constructive comments that helped us to improve our manuscript. K. Fontijn is supported by NERC grant NE/I013210/1. This work is a part of C. Vidal's PhD thesis (Institut de Physique du Globe de Paris). It has been partly funded by the Institut National des Sciences de l'Univers-Centre National de la Recherche Scientifique programme CT3-ALEA, projects ECRin 2013 and 2014, and INSU-CNRS Artemis 2014 for ^{14}C dating. This is IGP contribution 3550.

References

- Andreastuti SD (1999) Stratigraphy and geochemistry of Merapi volcano, central Java, Indonesia: implication for assessment of volcanic hazard. PhD thesis, University of Auckland
- Andreastuti SD, Alloway BV, Smith IEM (2000) A detailed tephrostratigraphic framework at Merapi Volcano, Central Java, Indonesia: implications for eruption predictions and hazard assessment. *J Volcanol Geotherm Res* 100:51–67
- Barbier B (2010) Bilan thermique et caractérisation géochimique de l'activité hydrothermale du volcan Rinjani (Lombok, Indonésie). PhD thesis, Université Libre de Bruxelles
- Bonadonna C, Costa A (2012) Estimating the volume of tephra deposits: a new simple strategy. *Geology* 40(5):415–418
- Bonadonna C, Costa A (2013) Plume height, volume, and classification of explosive volcanic eruptions based on the Weibull function. *Bull Volcanol* 75:742–762
- Bonadonna C, Houghton B (2005) Total grain-size distribution and volume of tephra-fall deposits. *Bull Volcanol* 67:441–456
- Bonadonna C, Ernst GGJ, Sparks RSJ (1998) Thickness variations and volume estimates of tephra fall deposits: the importance of particle Reynolds number. *J Volcanol Geotherm Res* 81:173–187
- Bonadonna C, Cioni R, Pistolesi M, Connor C, Scollo S, Pioli L, Rosi M (2013) Determination of the largest clast sizes of tephra deposits for the characterization of explosive eruptions: a study of the IAVCEI

- commission on tephra hazard modelling. *Bull Volcanol* 75(680):1–15. doi:10.1007/s00445-012-0680-3
- Branney MJ, Kokelaar P (2002) Pyroclastic density currents and the sedimentation of ignimbrites. *Geol Soc Lond Mem* 27:1–143
- Bull ID, Knicker H, Poirier N, Porter HC, Scott AC, Sparks RSJ, Richard P (2008) Evershed, biomolecular characteristics of an extensive tar layer generated during eruption of the Soufriere Hills volcano, Montserrat, West Indies. *Org Geochem* 39:1372–1383
- Bursik MI, Sparks RSJ, Gilbert JS, Carey SN (1992) Sedimentation of tephra by volcanic plumes: I. Theory and its comparison with a study of the Fogo A plinian deposit, Sao Miguel (Azores). *Bull Volcanol* 54:329–344
- Carazzo G, Kaminski E, Tait S (2008) On the rise of turbulent plumes: quantitative effects of variable entrainment for submarine hydrothermal vents, terrestrial and extra-terrestrial explosive volcanism. *J Geophys Res*. doi:10.1029/2007JB005458
- Carey SN, Sparks RSJ (1986) Quantitative models of the fallout and dispersal of tephra from volcanic eruption columns. *Bull Volcanol* 48:109–125
- Cole-Dai J, Ferris DG, Lanciki AL, Savarino J, Thiemens MH, McConnell JR (2013) Two likely stratospheric volcanic eruptions in the 1450s C.E. found in a bipolar, subannually dated 800 year ice core record. *J Geophys Res* 118:7459–7466. doi:10.1002/jgrd.50587
- Croweller HS, Arora B, Brown SK, Cottrell E, Deligne NI, Guerrero NO, Hobbs L, Kiyosugi K, Loughlin SC, Lowndes J, Nayemil M, Siebert L, Sparks RSJ, Takarada S, Venzke E (2012) Global database on large magnitude explosive volcanic eruptions (LaMEVE). *J Appl Volcanol* 1:4. <http://www.appliedvolc.com/content/1/1/4>
- Daggit ML, Mather TA, Pyle DM, Page S (2014) AshCalc—a new tool for the comparison of the exponential, power-law and Weibull models of tephra deposition. *J Appl Volcanol* 3:7
- Druitt TH, Calder ES, Cole PD, Hoblitt RP, Loughlin SC, Norton GE, Ritchie LJ, Sparks RS, Voight B (2002) Small-volume, highly mobile pyroclastic flows formed by rapid sedimentation from pyroclastic surges at Soufrière Hills volcano, Montserrat: an important volcanic hazard. In: Druitt TH, Kokelaar BP (eds) *The eruption of Soufrière Hills volcano, Montserrat, from 1995 to 1999: Mem Geol Soc Lond* 21, pp 263–280
- Engwell SL, Sparks RSJ, Aspinall WP (2013) Quantifying uncertainties in the measurement of tephra fall thickness. *J Appl Volcanol* 2:5
- Fierstein J, Nathenson M (1992) Another look at the calculation of fallout tephra volumes. *Bull Volcanol* 4:156–167
- Fontijn K, Costa F, Sutawidjaja I, Newhall CG, Herrin JS (2015) A five thousand year record of multiple highly explosive mafic eruptions from Gunung Agung (Bali, Indonesia): implications for eruption frequency and volcanic hazards. *Bull Volcanol*. doi:10.1007/s00445-015-0943-x
- Furukawa R, Takada A, Nasution A (2005) Caldera forming eruption of Rinjani volcano at 13th century, Lombok, Indonesia. In: *Abstracts Fall Meet Volcanol Soc Japan, Hokkaido, Japan*
- Furukawa R, Takada A, Nasution A, Taufiqurrohman R (2014) Eruptive sequence of Rinjani caldera, 13th century, Lombok, Indonesia. In: *Abstracts Japan Geosci Union Meet, Yokohama, Japan, 28 May–2 April 2014*
- Gao C, Oman L, Robock A, Stenchikov L (2008) Atmospheric volcanic loading derived from bipolar ice cores: accounting for the spatial distribution of volcanic deposition. *J Geophys Res*. doi:10.1029/2006JD007461
- Gennaretti F, Arseneault D, Nicault A, Perreault L, Bégin Y (2014) Volcano-induced regime shifts in millennial tree-ring chronologies from northeastern North America. *Proc Natl Acad Sci U S A* 111(28):10077–10082. doi:10.1073/pnas.1324220111
- Gerlach M, Westrich RH, Symonds RB (1996) Preeruption vapor in magma of the climactic Mount Pinatubo eruption: source of the giant stratospheric sulfur dioxide cloud. In: Newhall CG, Punongbayan RS (eds) *Fire and mud: eruptions and lahars of Mount Pinatubo, Philippines*. PHIVOLCS, Quezon City, Philippines and University of Washington Press, Seattle, pp 415–433
- Gertisser R (2001) *Gunung Merapi (Java, Indonesien): Eruptionsgeschichte und magmatische Evolution eines Hochrisiko-Vulkans*. PhD thesis, Universität Freiburg
- Gertisser R, Charbonnier SJ, Keller J, Quidelleur X (2012) The geological evolution of Merapi volcano, Central Java. *Bull Volcanol* 74:1213–1233. doi:10.1007/s00445-012-0591-3
- Global Volcanism Program (2014) *Bulletin*, Smithsonian Institution, Washington D.C. <http://www.volcano.si.edu/>. Accessed 31 Dec 2014
- Houghton BF, Wilson CJN, Smith RT, Gilbert JS (2000) Phreatoplinian eruptions. In: Sigurdsson H, Houghton BF, Rymer H, Stix J, McNutt S (eds) *Encyclopedia of volcanoes*, pp 513–525
- Houghton BF, Carey RJ, Rosenberg MD (2014) The 1800a Taupo eruption: “Ill wind” blows the ultraplinian type event down to plinian. *Geology* 42(5):459–461
- Kandlbauer J, Sparks RSJ (2014) New estimates of the 1815 Tambora eruption volume. *J Volcanol Geotherm Res*. doi:10.1016/j.jvolgeores.2014.08.020
- Lavigne F, Degeai JP, Komorowski JC, Guillet S, Robert V, Lahitte P, Oppenheimer C, Stoffel M, Vidal CM, Pratomo I, Wassmer P, Hajdas I, Sri Hadmoko D, de Bézilaz E (2013) Source of the great A.D. 1257 mystery eruption unveiled: Samalas volcano, Rinjani volcanic complex, Indonesia. *Proc Natl Acad Sci U S A*. doi:10.1073/pnas.13075201100
- Longpré MA, Stix J, Burkert C, Hansteen T, Kutterolf S (2014) Sulfur budget and global climate impact of the A.D. 1835 eruption of Cosigüina volcano, Nicaragua. *Geophys Res Lett* 41. doi:10.1002/2014GL061205
- Miller CF, Wark DA (2008) Supervolcanoes and their explosive supereruptions. *Elements* 4(1):11–16
- Miller GH, Geirsdóttir A, Zhong Y, Larsen DJ, Otto-Bliesner BL, Holland MM, Bailey DA, Refsnider KA, Lehman SJ, Southon JR, Anderson C, Björnsson H, Thordarson T (2012) Abrupt onset of the Little Ice Age triggered by volcanism and sustained by sea-ice/ocean feedbacks. *Geophys Res Lett* 39, L0270810. doi:10.1029/2011GL050168
- Nasution A, Takada A, Rosgandika M (2004) The volcanic activity of Rinjani, Lombok Island, Indonesia, during the last thousand years, viewed from 14C datings. In: *Abstracts of the Convention Bandung 2004, The 33rd annual convention & exhibition, 29 Nov–1 Oct 2004, Bandung, Indonesia*
- Nasution A, Takada A, Udibowo WD, Hutasoit L (2010) Rinjani and Propok volcanics as a heat sources of geothermal prospects from eastern Lombok, Indonesia. *Jurnal Geoplaka* 5(1):1–9
- Newhall CG, Dzurisin D (1989) Historical unrest at large calderas of the world. *US Geol Surv Prof Pap* 1855:1–1109
- Newhall CG, Self S (1982) The Volcanic Explosivity Index (VEI): an estimate of explosive magnitude for historical volcanism. *J Geophys Res Oceans Atm* 87:1231–1238
- Newhall CG, Bronto S, Alloway B, Banks NG, Bahar I, Del Marmol MA, Hadisantono RD, Holcomb RT, McGeehin J, Miksic JN, Rubin M, Sayudi SD, Sukhyar R, Andreastuti S, Tilling RI, Torley R, Trimble D, Wirakusumah AD (2000) 10,000 years of explosive eruptions of Merapi Volcano, Central Java: archaeological and modern implications. *J Volcanol Geotherm Res* 100:9–50
- Oppenheimer C (2003) Ice core and palaeoclimatic evidence for the timing and nature of the great mid-13th century volcanic eruption. *Int J Climatol* 23(4):417–426
- Palais JM, Germani MS, Zielinski GA (1992) Interhemispheric transport of volcanic ash from a 1259 A.D. volcanic eruption to the Greenland and Antarctic ice sheets. *Geophys Res Lett* 19(8):801–804

- Plummer CT, Curran MAJ, van Ommen TD, Rasmussen SO, Moy AD, Vance TR, Clausen HB, Vinther BM, Mayewski PA (2012) An independently dated 2000-yr volcanic record from Law Dome, East Antarctica, including a new perspective on the dating of the 1450s CE eruption of Kuwae, Vanuatu. *Clim Past* 8:1929–1940
- Pyle DM (1989) The thickness, volume and grainsize of tephra fall deposits. *Bull Volcanol* 51(1):1–15
- Pyle DM (1995) Assessment of the minimum volume of tephra fall deposits. *J Volcanol Geotherm Res* 69(3–4):379–382
- Pyle DM (2000) Sizes of volcanic eruptions. In: Sigurdsson H, Houghton B, Reimer H, Stix J, McNutt S (eds) *Encyclopedia of volcanoes*. Academic, San Diego, pp 263–269
- Robock A (2000) Volcanic eruptions and climate. *Rev Geophys* 38:191–219. doi:10.1029/1998RG000054
- Rodysill JR, Russell JM, Bijaksana S, Brown ET, Safiuddin LO, Eggermont H (2012) A paleolimnological record of rainfall and drought from East Java, Indonesia during the last 1,400 years. *J Paleolimnol* 47:125–139
- Rodysill JR, Russell JM, Crausbay SD, Bijaksana S, Vuille M, Edwards RL, Cheng H (2013) A severe drought during the last millennium in East Java, Indonesia. *Quat Sci Rev* 80:102–111
- Schmidt A, Robock A (2015) Volcanism, the atmosphere and climate through time. In: Schmidt A, Fristad KE and Elkins-Tanton LT (eds) *Volcanism and global environmental change*. Cambridge Univ Press 195–227
- Schneider DP, Ammann CM, Otto-Bliesner BL, Kaufman DS (2009) Climate response to large, high-latitude and low-latitude volcanic eruptions in the Community Climate System model. *J Geophys Res* 114, D15101
- Scott AC, Sparks RSJ, Bull ID, Knicker H, Evershed RP (2008) Temperature proxy data and their significance for the understanding of pyroclastic density currents. *Geology* 36(2):143–146
- Self S (2006) The effects and consequences of very large explosive volcanic eruptions. *Phil Trans R Soc A* 364:2073–2097. doi:10.1098/rsta.2006.1814
- Self S, Rampino MR, Newton MS, Wolff JA (1984) Volcanological study of the great Tambora eruption of 1815. *Geology* 12:659–663
- Self S, Gertisser R, Thordarson T, Rampino MR, Wolff JA (2004) Magma volume, volatile emissions, and stratospheric aerosols from the 1815 eruption of Tambora. *Geophys Res Lett* 31, L20608. doi:10.1029/2004GL020925
- Sheridan MF, Wohletz KH (1983) Hydrovolcanism: basic considerations and review. *J Volcanol Geotherm Res* 17:1–29
- Sigl M, McConnell JR, Layman L, Maselli O, McGwire K, Pasteris D, Dahl-Jensen D, Steffensen JP, Vinther B, Edwards R, Mulvaney R, Kipfstuhl S (2013) A new bipolar ice core record of volcanism from WAIS Divide and NEEM and implications for climate forcing of the last 2000 years. *J Geophys Res Atmos* 118:1151–1169. doi:10.1029/2012JD018603
- Sigl M, McConnell JR, Toohey M, Curran M, Das SB, Edwards R, Isaksson E, Kawamura K, Kipfstuhl S, Kruger K, Layman L, Maselli OJ, Motizuki Y, Motoyama H, Pasteris DR, Severi M (2014) Insights from Antarctica on volcanic forcing during the Common Era. *Nat Clim Chang* 4:693–697
- Sigurdsson H, Carey S (1989) Plinian and co-ignimbrite tephra fall from the 1815 eruption of Tambora volcano. *Bull Volcanol* 51:243–270
- Simons WJF, Socquet A, Vigny C, Ambrosius BAC, Haji Abu S, Promthong C, Subarya C, Sarsito DA, Matheussen S, Morgan P, Spakman W (2007) A decade of GPS in Southeast Asia: resolving Sundaland motion and boundaries. *J Geophys Res* 112, B06420. doi:10.1029/2005JB003868
- Sparks RSJ (1986) The dimensions and dynamics of volcanic eruption columns. *Bull Volcanol* 48:13–15
- Sparks RSJ, Walker GPL (1977) The significance of vitric-enriched air-fall ashes associated with crystal-enriched ignimbrites. *J Volcanol Geotherm Res* 2:329–341
- Sparks RSJ, Wilson L (1976) A model for the formation of ignimbrite by gravitational column collapse. *J Geol Soc Lond* 132:441–451
- Sparks RSJ, Barclay J, Calder ES, Herd RA, Komorowski JC, Luckett R, Norton GE, Ritchie LJ, Voight B, Woods AW (2002) Generation of a debris avalanche and violent pyroclastic density current on 26 December (Boxing Day) 1997 at Soufriere Hills volcano, Montserrat. In: Druitt TH, Kokelaar BP (eds) *Geol Soc Lond, Mem* 21:409–434
- Stothers RB (2000) Climatic and demographic consequences of the massive eruption of 1258. *Clim Chang* 45(2):361–374
- Sulpizio R (2005) Three empirical methods for the calculation of distal volume of tephra-fall deposits. *J Volcanol Geotherm Res* 145(3–4):315–336
- Takada A, Nasution A, Rosgandika M (2003) Eruptive history during the last 10ky for the caldera-forming eruption of Rinjani volcano. In: Abstracts of Japan Earth and Planet Sci Joint Meet, Chiba, Japan, 26–29 May 2003
- Timmreck C (2012) Modelling the climatic effect of large explosive volcanic eruptions. *WIREs Clim Chang*. doi:10.1002/wcc.192
- Vidal CM, Métrich N, Komorowski JC, Pratomo I, Lavigne F, Suroño (2013) Insights into the magmatic processes leading to the Holocene caldera eruption of Rinjani, Indonesia. *Goldschmidt 2013 International Conference, Florence, Italy, 25–30 August 2013, Mineral Mag* 77(5):2413
- Vidal C, Komorowski J-C, Métrich N, Pratomo I, Kartadinata N, Lavigne F, Prambada O, Fontijn K, Rodysill J, Michel A, Kuhn W, Suroño (2015) Eruptive dynamics of a major plinian eruption with evidence of global impact: the recently discovered Samalas 1257 AD eruption (Rinjani volcanic complex, Lombok, Indonesia). In: Abstracts of Volcanoes, Climate, and Society, Bicentenary of the great Tambora eruption Conference, 7–11 April 2015, Bern, Switzerland
- Voight B, Komorowski JC, Norton G, Belousov A, Belousova M, Boudon G, Francis P, Franz W, Sparks S, Young S (2002) The 1997 Boxing Day sector collapse and debris avalanche, Soufriere Hills Volcano, Montserrat, B.W.I. In: Druitt, T., Kokelaar, B.P. (Eds.), *The eruption of Soufriere Hills volcano, Montserrat, from 1995–1999: Mem Geol Soc Lond* 21, pp 363–407
- Walker GPL (1973) Explosive volcanic eruptions—a new classification scheme. *Geol Rundsch* 62:431–446
- Walker GPL (1980) The Taupo Pumice: product of the most powerful known (Ultraplinian) eruption? *J Volcanol Geotherm Res* 8:69–94
- Walker GPL (1981) The Waimihia and Hatepe plinian deposits from the rhyolitic Taupo volcanic Centre. *N Z J Geol Geophys* 24:305–324
- Williams SN, Self S (1983) The October 1902 plinian eruption of Santa Maria volcano, Guatemala. *J Volcanol Geotherm Res* 16:36–56
- Witter JB, Self S (2007) The Kuwae (Vanuatu) eruption of AD 1452: potential magnitude and volatile release. *Bull Volcanol* 69:301–318. doi:10.1007/s00445-006-0075-4
- Woods A, Wohletz K (1991) Dimensions and dynamics of co-ignimbrite eruption columns. *Nature* 350:225–227
- Young SR (1990) Physical volcanology of Holocene airfall deposits from Mt Mazama, Crater Lake, Oregon. PhD thesis, University of Lancaster
- Zielinski GA, Mayewski PA, Meeker LD, Whitlow S, Twickler MS, Morrison M, Meese D, Alley RB, Gow AJ (1994) Record of volcanism since 7000 B.C. from the GISP2 Greenland ice core and implication for the volcano-climate system. *Science* 264:948–952